SANDIA REPORT
SAND2012-0902
Unlimited Release
Printed February 2012

Composite Materials for Hazard Mitigation of Reactive Metal Hydrides

Joseph W. Pratt, Joseph G. Cordaro, George B. Sartor, Craig L. Reeder, and Daniel E. Dedrick

Prepared by
Sandia National Laboratories
Albuquerque, New Mexico 87185 and Livermore, California 94550

Sandia National Laboratories is a multi-program laboratory managed and operated by Sandia Corporation, a wholly owned subsidiary of Lockheed Martin Corporation, for the U.S. Department of Energy's National Nuclear Security Administration under contract DE-AC04-94AL85000.

Issued by Sandia National Laboratories, operated for the United States Department of Energy by Sandia Corporation.

Available to DOE and DOE contractors from
U.S. Department of Energy
Office of Scientific and Technical Information
P.O. Box 62
Oak Ridge, TN 37831

Telephone: (865) 576-8401
Facsimile: (865) 576-5728
E-Mail: reports@adonis.osti.gov
Online ordering: http://www.osti.gov/bridge

Available to the public from
U.S. Department of Commerce
National Technical Information Service
5285 Port Royal Rd.
Springfield, VA 22161

Telephone: (800) 553-6847
Facsimile: (703) 605-6900
E-Mail: orders@ntis.fedworld.gov
Online order: http://www.ntis.gov/help/ordermethods.asp?loc=7-4-0#online

SAND2012-0902
Unlimited Release
Printed February 2012

Composite Materials for Hazard Mitigation of Reactive Metal Hydrides

Joseph W. Pratt[1], Joseph G. Cordaro[2], George B. Sartor[1], Craig L. Reeder[2], and Daniel E. Dedrick[3]

[1]Energy Systems Engineering & Analysis (8366)
[2]Materials Chemistry (8223)
[3]Hydrogen and Combustion Technology (8367)
Sandia National Laboratories
P.O. Box 969
Livermore, California, 94551

Abstract

In an attempt to mitigate the hazards associated with storing large quantities of reactive metal hydrides, polymer composite materials were synthesized and tested under simulated usage and accident conditions.

The composites were made by polymerizing vinyl monomers using free-radical polymerization chemistry, in the presence of the metal hydride. Composites with vinyl-containing siloxane oligomers were also polymerized with and without added styrene and divinyl benzene.

Hydrogen capacity measurements revealed that addition of the polymer to the metal hydride reduced the inherent hydrogen storage capacity of the material. The composites were found to be initially effective at reducing the amount of heat released during oxidation. However, upon cycling the composites, the mitigating behavior was lost.

While the polymer composites we investigated have mitigating potential and are physically robust, they undergo a chemical change upon cycling that makes them subsequently ineffective at mitigating heat release upon oxidation of the metal hydride.

Acknowledgements

The authors would like to thank the following people who participated in this project:

- Ned Stetson (U.S. Department of Energy) for sponsorship and support of the project.
- Ken Stewart (Sandia) for building the flow-through calorimeter and cycling test stations.
- Isidro Ruvalcaba, Jr. (Sandia) for qualitative experiments on the interaction of sodium alanate with water.
- Terry Johnson (Sandia) for sharing his expertise and knowledge of metal hydrides, and sodium alanate in particular.
- Marcina Moreno (Sandia) for programmatic assistance.
- John Khalil (United Technologies Research Corp) for insight into the hazards of reactive metal hydrides and real-world accident scenario experiments.

Summary

In an attempt to mitigate and/or manage hazards associated with storing bulk quantities of reactive metal hydrides, polymer composite materials (a mixture of a mitigating polymer and a metal hydride) were synthesized and tested under simulated usage and accident conditions. Mitigating the hazards associated with reactive metal hydrides during an accident while finding a way to keep the original capability of the active material intact during normal use has been the focus of this work.

These composites were made by polymerizing vinyl monomers using free-radical polymerization chemistry, in the presence of the metal hydride, in this case a prepared sodium alanate (chosen as a representative reactive metal hydride). It was found that the polymerization of styrene and divinyl benzene could be initiated using AIBN in toluene at 70 °C. The resulting composite materials can be either hard or brittle solids depending on the cross-linking density. Thermal decomposition of these styrene-based composite materials is lower than neat polystyrene indicating that the chemical nature of the polymer is affected by the formation of the composite. The char-forming nature of cross-linked polystyrene is low and therefore, not an ideal polymer for hazard mitigation.

To obtain composite materials containing a polymer with higher char-forming potential, siloxane-based monomers were investigated. Four vinyl-containing siloxane oligomers were polymerized with and without added styrene and divinyl benzene. Like the styrene materials, these composite materials exhibited thermal decomposition behavior significantly different than the neat polymers. Specifically, the thermal decomposition temperature was shifted approximately 100 °C lower than the neat polymer signifying a major chemical change to the polymer network. Thermal analysis of the cycled samples was performed on the siloxane-based composite materials. It was found that after 30 cycles the siloxane-containing polymer composite material has similar TGA/DSC-MS traces as the virgin composite material indicating that the polymer is physically intact upon cycling.

Hydrogen capacity measurements revealed that addition of the polymer to the metal hydride in the form of a composite material reduced the inherent hydrogen storage capacity of the material. This reduction in capacity was observed to be independent of the amount of charge/discharge cycles except for the composites containing siloxane, which showed less of an impact on hydrogen storage capacity as it was cycled further. While the reason for this is not clear, it may be due to a chemically stabilizing effect of the siloxane on the metal hydride.

Flow-through calorimetry was used to characterize the mitigating effectiveness of the different composites relative to the neat (no polymer) material. The composites were found to be initially effective at reducing the amount of heat released during oxidation, and the best performing material was the siloxane-containing composite which reduced the heat release to less than 50% of the value of the neat material. However, upon cycling the composites, all mitigating behavior was lost.

The combined results of the flow-through calorimetry, hydrogen capacity, and thermogravimetric analysis tests lead to the proposed conclusion that while the polymer composites have mitigating potential and are physically robust under cycling, they undergo a chemical change upon cycling that makes them ineffective at mitigating heat release upon oxidation of the metal hydride.

Contents

Figures

Tables

Nomenclature

Acronyms

AIBN	Azobisisobutyronitrile
DSC	Differential scanning calorimetry
DVB	Divinylbenzene
EDS	Energy dispersive spectrum
M-H	Metal-hydride as prepared
MS	Mass spectrometer
PI	Proportional-Integral
RGA	Residual Gas Analyzer
sccm	Standard cubic centimeters per minute
SEM	Scanning electron microscope
SLPM	Standard Liters Per Minute
St	Styrene
TGA	Thermal gravimetric analysis
UHP	Ultra High Purity (99.999% pure)

Symbols

A	Area
b	A constant
C_p	Specific heat at constant pressure
h	Effective heat transfer coefficient
m	Mass
$\dot{m}$	Mass flow rate of gas
MW	Molecular weight
P	Pressure
Q	Quantity of heat absorbed/lost
$\dot{Q}$	Rate of heat absorbed/lost
R	Universal gas constant
t	Time
T	Temperature
V	Volume

Greek Letters

Δ	A change
ρ	Density

1 Introduction

For most applications of hydrogen, the hydrogen storage system is desired to be as small and/or light as possible. Reversible metal hydrides have high volumetric (kJ/L) and gravimetric (kJ/kg) energy densities and have the potential meet this need. One potential drawback to these materials is that some have been shown to be reactive with oxygen and/or water, including sodium alanate ($NaAlH_4$) [1, 2], alane (AlH_3) [3], destabilized lithium borohydride ($2LiBH_4$:MgH_2) [4], and magnesium amide/ lithium hydride mixtures ($Mg(NH_2)_2$ + LiH) [5]. This is typically not a concern, because during preparation of these materials and assembly of hydrogen storage systems recommendations have been proposed to prevent hazardous situations [6]. Much like a sealed battery system, once these systems are manufactured, good engineering design prevent the exposure of the materials to air and water, minimizing any additional hazard to the user.

However, risk analysis of hydrogen storage system use has revealed that there may be situations where the material is unintentionally exposed to air or water [7]. This could be a tank breach or rupture, or water/air intrusion into the vessel through leaks or by filling with contaminated hydrogen. Therefore, to enable widespread use of these promising materials it is necessary to plan for these accidents by finding ways to minimize the resulting reaction to a non-hazardous level.

For several years, Sandia National Laboratories has been exploring different aspects of hazard mitigation of reactive metal hydrides, using sodium alanate as a representative active material [1, 8-16]. Sodium alanate readily charges and discharges hydrogen gas between 120 and 180 °C. The elementary reaction steps are as follows:

$$NaAlH_4 \leftrightarrow \frac{1}{3}Na_3AlH_6 + \frac{2}{3}Al + H_2 \quad (1)$$

$$Na_3AlH_6 \leftrightarrow 3NaH + Al + \frac{3}{2}H_2 \quad (2)$$

The reaction is made reversible though catalysis with titanium by various means including ball milling. While much energy can be stored in the form of chemical bonds, and utilized to generate electricity, metal hydrides such as $NaAlH_4$ are also reactive with water and oxygen.

Mitigating the hazards associated with solid sodium alanate during an accident while finding a way to keep the original capability of the active material intact during normal use has been the focus of this work. To do this we have been investigating a method of creating a homogeneous composite material of active and normally inactive materials, through polymerization and cross-linking of the inactive material (i.e., a polymer) in the presence of the active material ($NaAlH_4$). The bulk of our work focused on cross-linked polymer styrene based composite materials but we also investigated some hybrid polysiloxane/styrene composite materials because of their higher char-formation.

The goal of creating a polymer/metal-hydride composite material was threefold. First, a porous, light weight polymer could function as a structural framework for a metal hydride powder. The polymer pore-size can be tuned by varying the cross-linking density and amount of sacrificial porogen (or solvent). Ideally, the structural support of the polymer would prevent metal hydride particles from packing tightly

after long-term cycling, improve gas flow, and possibly suppress particle dispersion in the event of a breach-in-tank.

Second, a polymer/metal-hydride composite material could act as a fire-suppressant in the event of a breach-in-tank. Polymers with certain functional groups are known fire-suppressants by the action of char formation or through the sequestration of free-radicals formed within the flame. A polymer composite material has the potential to form a char around the reactive metal hydride in the event of a breach-in-tank, limiting the supply of oxygen or water, which would kinetically retard the oxidation reactions of the metal hydride.

Lastly, though not explored thoroughly, a porous polymer network has the ability to interact with the guest metal-hydride material to alter the kinetics of hydrogen cycling. It is known that catalytic amounts of titanium atoms/clusters alter the kinetics of equations (1)-(2), lowering the activation energy for the release of hydrogen. It is possible that a high-surface area polymer network decorated with the appropriate functional sites could similarly influence the kinetic behavior of sodium alanate hydrogen cycling.

In searching for polymer formulations that would meet these goals we investigated several different inactive materials and for each one we evaluated its overall effectiveness by assessing:

1. The degree to which the polymer mitigates the reactivity of the active material when exposed to oxygen.
2. The impact of including the polymer in the composite on the ability of the active material to effectively adsorb, store, and release hydrogen.
3. The durability of the polymer with respect to realistic usage conditions.

This report describes the results of the composite material development and evaluation effort. While some of this work has already been shown in the various presentations and annual reports for the Department of Energy referenced above, when appropriate we include this information again to provide a comprehensive description of our work on using composite materials to mitigate the hazards of reactive metal hydrides.

2 Experimental Methods

The setup and method of the three experimental components in this study are described in this section. The first section describes the methods used in synthesizing and characterizing the polymers and composite materials. The next section describes the mitigation tests, measured by heat release. The last section describes the capacity and durability experiments.

2.1 Composite Materials Development and Synthesis

A cross-linked polymer network was chosen as the target scaffold for the metal hydride. Additives or other small molecules that could have fire-suppressant properties were avoided because with long-term cycling they might phase-separate from the metal-hydride and become ineffective. In order to make a robust polymer/metal hydride composite material, it was decided that monomers should be polymerized in situ with the sodium alanate. Since metal hydrides are strong reducing agents and react rapidly with protic hydrogens, halogens, ketones/aldehydes, halides, and a host of other organic functional groups and metals, monomers had to be chosen carefully. Similarly, the polymerization route had to be tolerant to the strongly reducing alanate. Cationic and most transition metal-mediated polymerizations were therefore avoided. The most obvious route for making polymer/metal-hydride materials was to employ free radical polymerization of styrene and divinyl benzene in toluene using AIBN as initiator.

Materials: All composite materials were made inside an argon-filled glove box with oxygen and water levels below 1 ppm. Styrene (Acros) and divinyl benzene (Acros) were passed through a basic alumina column and stored at –38 °C. AIBN (Aldrich) was recrystallized from methanol and stored at –38 °C. Toluene was purified using Vacuum-Atmosphere's push-solvent system and stored over 3Å molecular sieves. Sodium aluminum hydride ($NaAlH_4$), or sodium alanate (Aldrich) was used as received. The discharged metal-hydride (M-H) used for all composites was made by ball-milling NaH, Al, and $TiCl_3$ and mixing with natural graphite. This mixture has been previously characterized and is the standard hydrogen storage material used at Sandia National Laboratories for large-scale experiments [17, 18]. Four Siloxanes were purchased from Gelest, Inc., degassed and stored inside the glove box.

Synthesis: Composite materials were made by combining a known amount of metal-hydride with a stock solution of monomers and AIBN in an appropriate reaction vessel (usually a 20-mL scintillation vial with a cap). The mixture was then stirred or shaken to fully wet the M-H. Enough toluene was added to ensure that the solid M-H was completely wet but without excess solvent above the solid. The vessel was then sealed and heated to 70 °C for 24 hours. Typically, a stock solution of the monomers plus AIBN was heated in a parallel reaction vessel to compare with the composite material. After 24 h, the vessel was opened and the toluene allowed to evaporate within the glove box. After an additional 24 – 48 h at 70 °C, the solid was put under high vacuum to remove any residual toluene.

Characterization: Composite materials were characterized by thermal gravimetric analysis (TGA) using a Mettler-Toledo TGA/DSC 1. This instrument allows for simultaneous collection of weight loss and heat flow in and out of a sample compared to a reference pan. Samples were characterized from 50 – 500 °C with a ramp rate of 10 °C/min under 40 mL/min flow of argon. The off-gases generated during thermal decomposition were analyzed using a Pfeiffer mass spectrometer. Composite materials were analyzed

for weight loss both as virgin composite material (uncycled) and after cycling or flow through experiments.

2.2 Heat Release

A flow-through calorimeter was used to measure the heat release of the material when exposed to oxygen. A simplified schematic is shown in Figure 1 and a picture of the test bench is in Figure 2. The material to be tested is put into the cylindrical reaction vessel, a drawing of which is shown in Figure 3 and pictures in Figure 4, which has an internal radius of 0.203 inches (5.16 mm). Nominally 360 mg of material is added to the vessel for each test, and is slightly "tap" compacted to a nominal depth of 0.170 inches (4.32 mm), giving a target density of 998 kg/m^3 for each test. The material is contained within the volume by a 0.2 μm frit on the inlet and outlet. All active material handling is done within an Argon-filled glove box (see Figure 5). K-type thermocouples are used to measure the temperature of the material at various radial positions around the vessel: the center (r = 0 inches), midpoint (r = 0.102 inches / 2.59 mm), and edge (r = 0.203 inches / 5.16 mm). The arrangement of the thermocouples can be seen in Figure 4.

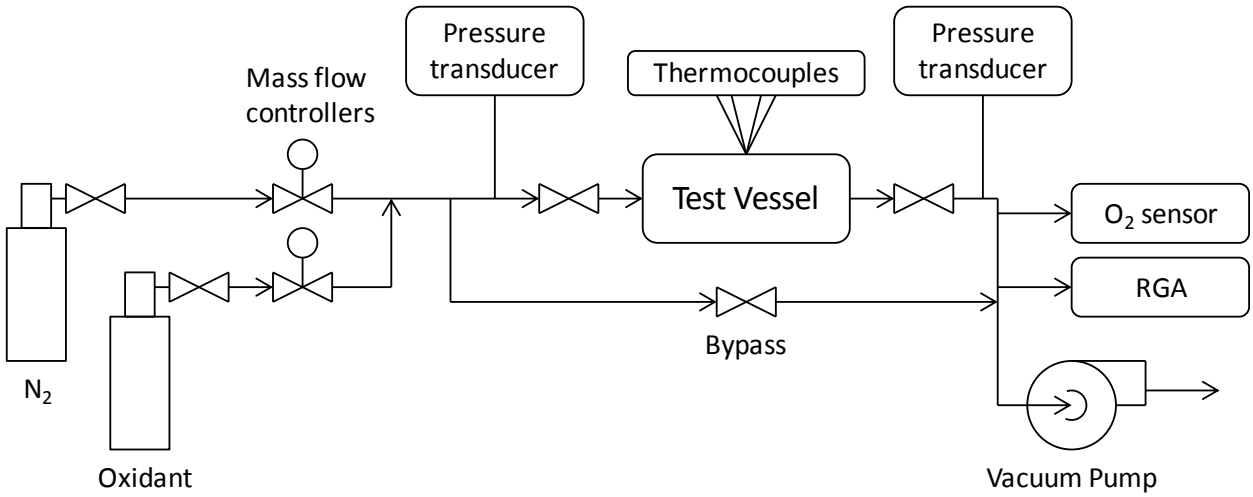

Figure 1: Simplified schematic of the flow-through calorimeter and permeability test bench.

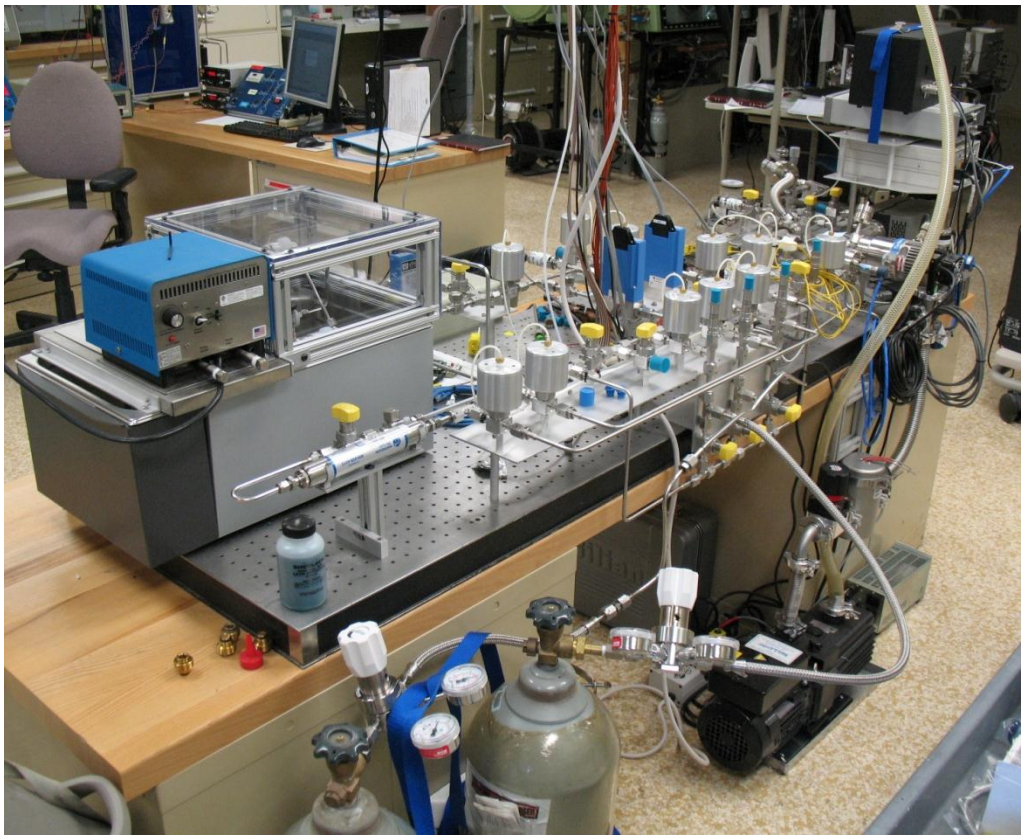

Figure 2: Flow-through calorimetry test bench.

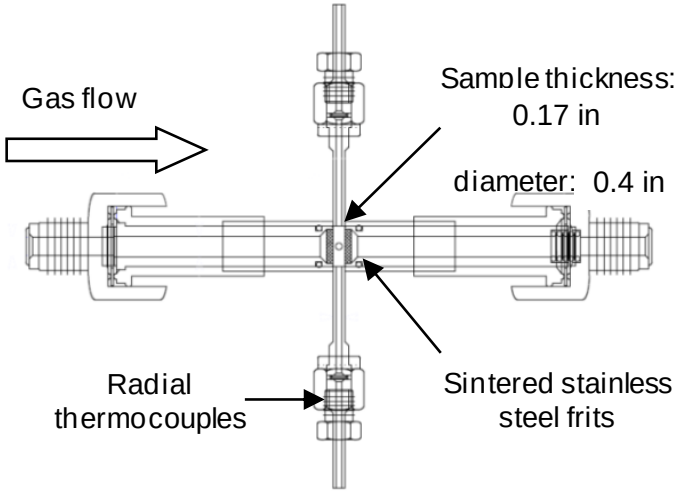

Figure 3: Side-view drawing of the sample holder for the flow-through calorimetry.

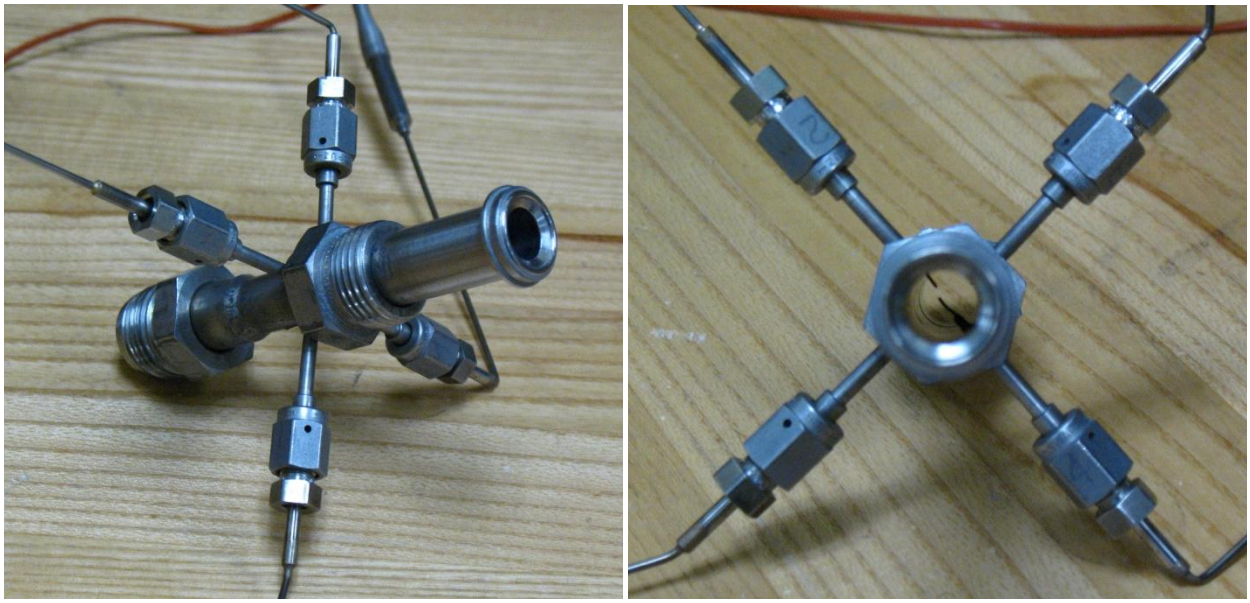

Figure 4: Sample holder for the flow-through calorimetry experiment. Axial view (right picture) shows the thermocouples that penetrate the sample to the center (from the bottom right) and to the midpoint radius (from the upper left). The other two thermocouples are flush with the sample holder inside wall.

Figure 5: Argon-filled glovebox used for finished-material handling and testing preparation.

A timeline of a representative test is shown in Figure 6. Upon starting a test, the system is brought to vacuum to evacuate any contaminants that may be left from a previous test. The sample is opened to the system and it is also evacuated. Then 0.1 SLPM of ultra-high purity (UHP) nitrogen (99.999%) is flowed (mass flow controllers: Matheson 8270 series) through the sample and the backpressure is adjusted to maintain a nominal pressure of 17 psia at its outlet. During this time the residual gas analyzer (RGA, Stanford Research Systems CIS200) and oxygen sensor (Oxigraf O2L) are monitored to see if any contaminants are still present, and the sample thermocouples are checked to see whether any unintended reaction takes place in the sample. If either of these events is detected, the test is aborted and the sample is discarded. The system is left to stabilize at this condition for about five minutes.

Pressure is measured upstream and downstream with transducers (MKS Inst. 870B Micro-Baratron), and all temperatures, flows, and pressures are continuously recorded through a data acquisition system. Nitrogen is flowed at various rates in order to estimate permeability (not detailed in this report). These tests last for approximately another 30 minutes. Once these tests are complete, the nitrogen is again set to 0.1 SLPM and the sample is heated with an external heat tape from room temperature to a

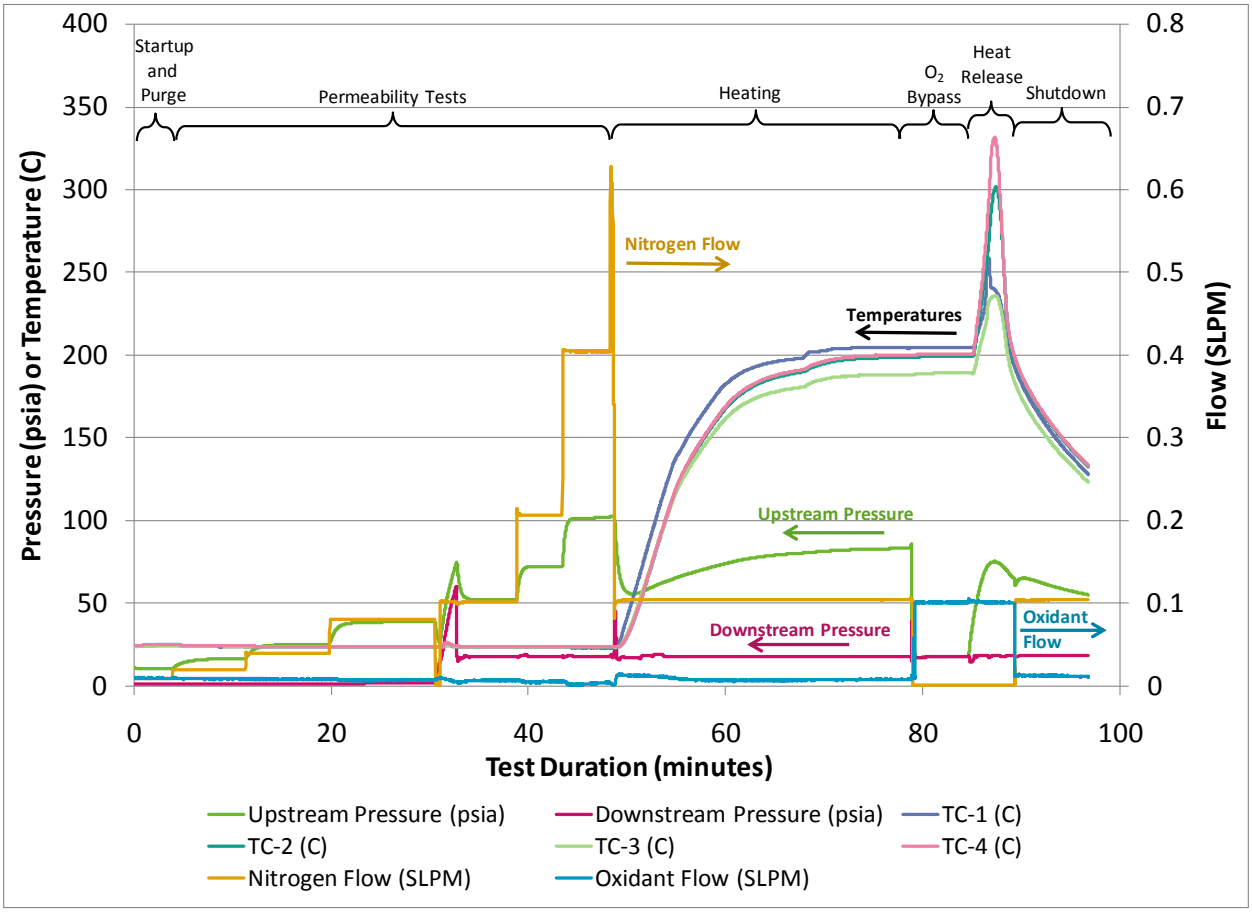

Figure 6: Overview of a typical heat release and permeability test run. This particular test was dated 2011-06-13 (see Table 5).

nominal temperature of 200 °C and allowed to stabilize. A copper jacket between the heat tape and sample holder is used to provide even heat distribution. The heating portion of the test typically takes 25-30 minutes.

At this point the nitrogen is stopped and the sample is isolated. Oxidation gas (24% O_2, 1% He (as tracer), balance N_2) is flowed through the sample bypass at 0.1 SLPM. The system is allowed to stabilize and this condition is held until the correct amount of oxygen is detected by the RGA and oxygen analyzer (typically 3-5 minutes). Then the sample is opened and the bypass is closed, sending oxidation gas through the sample. The reaction is monitored through the increase and subsequent decrease of sample temperatures, and also the composition of gases exiting the sample. As soon as the temperature begins to rise the heating tape becomes inactive due to its PI control, and after all the sample temperatures peak the heaters are manually turned off. Once the temperatures decreases below 200 °C, the oxidation gas is turned off and nitrogen at 0.1 SLPM is flowed, to assist in cooling down the system for shutdown. The entire oxidation and heat release portion of the test typically lasts less than five minutes.

2.3 Hydrogen Capacity

Hydrogen storage capacity was measured by an adsorption/desorption kinetics cycling station / Sievert apparatus, a simplified schematic of which is shown in Figure 7 with a picture in Figure 8. The material to be tested, nominally 2 g, is put into the vessel, a section of stainless steel tube. The vessel is dead-ended, with a 0.2 μm frit on the open end to allow the test gas (H_2) to pass in and out while keeping the material in the vessel. This frit is backed up by a 60 μm frit in case any material becomes loose during fabrication and a 0.5 μm frit where the vessel connects to Valve 5 to keep the system free of any powder that may leak by during cycling.

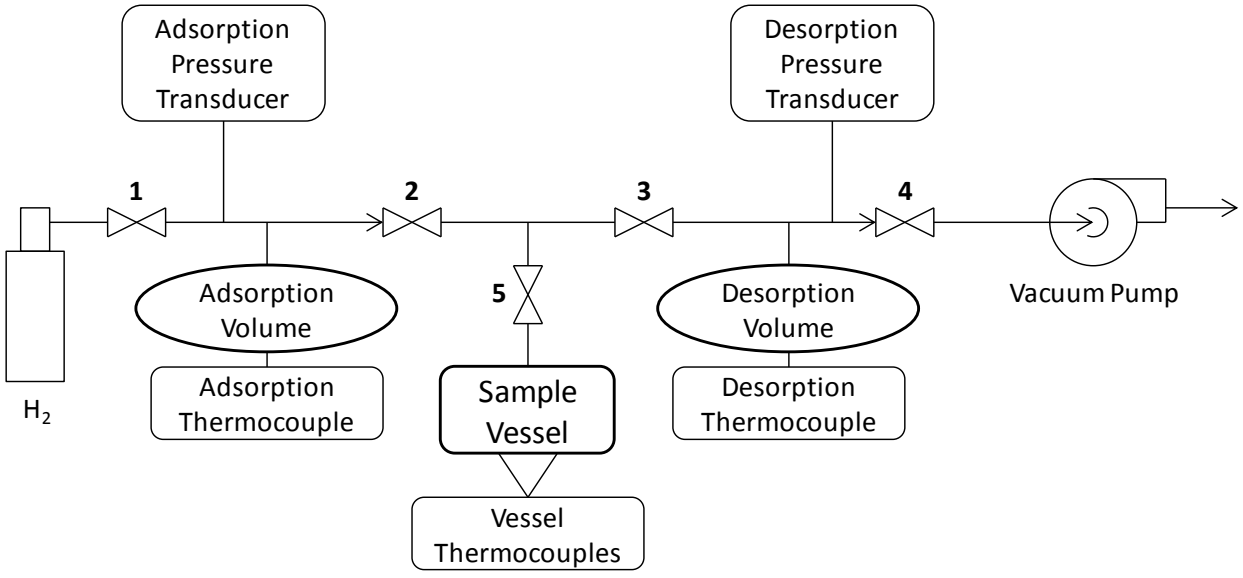

Figure 7: Simplified schematic of the automatic kinetics/cycling station. There are two identical stations that share the same hydrogen supply and vacuum pump, although only one is shown here.

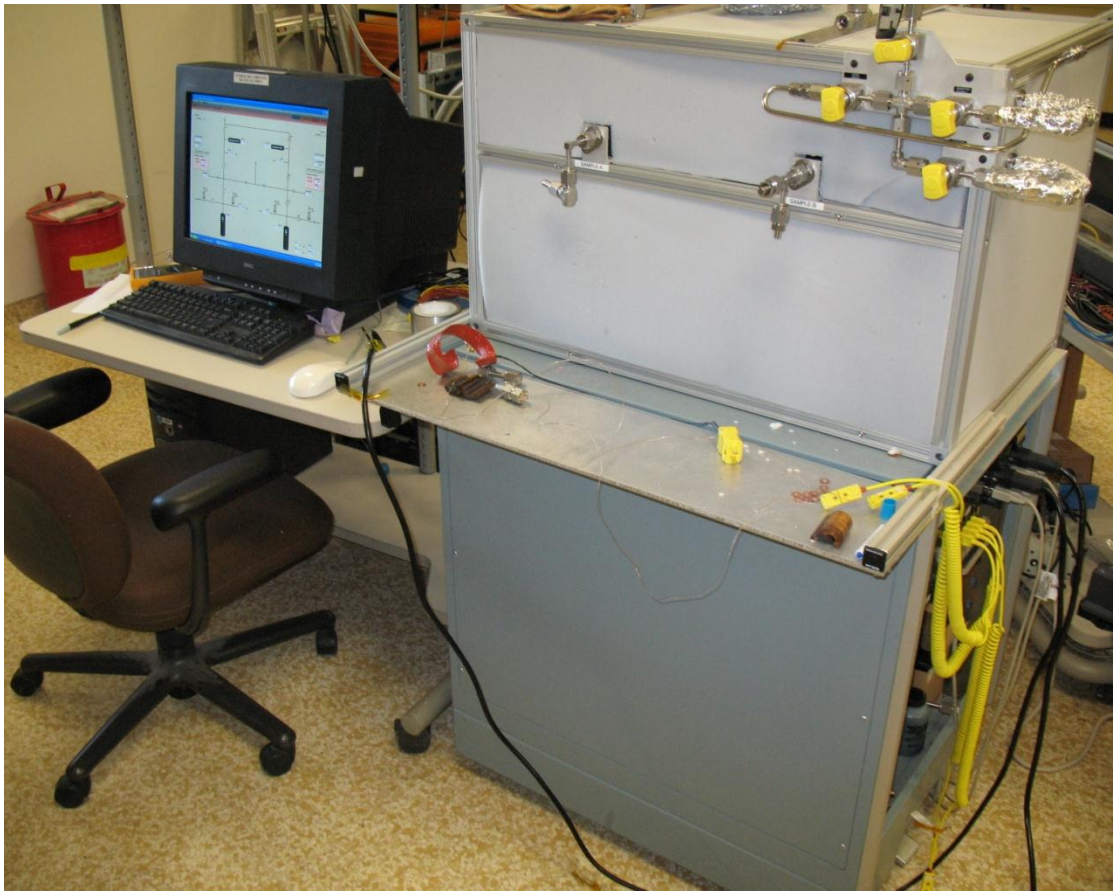

Figure 8: Picture of the kinetics/cycling station. The valves and adsorption/desorption volumes shown in Figure 7 are hidden in the enclosure.

Prior to beginning a test, Valves 3 and 4 are opened and the system is vacuum-purged to remove any contaminants that may be present. While under vacuum, Valve 5 (connecting the sample vessel to the system) is opened and the vessel is brought to vacuum as well. Valve 4 is then closed, isolating the system from the vacuum pump. With Valves 3 and 5 open, the sample is heated to nominally 190 °C and held for 60 minutes for an initial desorption of any hydrogen that may be present in the test material. The temperature and time are chosen based on the desorption kinetics, ensuring that all hydrogen is desorbed during this time. After this time, Valve 4 is opened and the system downstream of Valve 2 is brought to vacuum.

The actual capacity testing begins after this initial desorption. Valves 1-4 are closed (Valve 5 remains open for the remainder of the test) and the sample is brought to a nominal 145 °C. Valve 1 is opened, charging the Adsorption Volume with hydrogen at nominally 1,900 psig (131 bar). Valve 1 is closed and the amount of hydrogen trapped between Valve 1 and Valve 2 can be calculated based on the readings of the Adsorption Pressure Transducer and Adsorption Thermocouple (see the Data Analysis section). Valve 2 is opened, and the system is held in this state for 30 minutes, allowing enough time for the material to become fully adsorbed with hydrogen.

Now, desorption begins. Valve 2 is closed followed by Valve 3 opening, and the sample is heated to 190 °C. As hydrogen is desorbed form the sample, the pressure and temperature in the Desorption Volume rise, and the amount of hydrogen desorbed can be calculated (see the Data Analysis section). The sample is held in this state for 60 minutes to ensure complete desorption of the hydrogen. This concludes one cycle, and the next cycle begins with an adsorption (see previous paragraph) and repeated as many times as needed. The pressure and temperature data is recorded during the entire run. When no more cycles are to be attempted, the test is finished and the vessel is cooled to ambient temperature.

3 Data Analysis

This section describes the methods used in analyzing the experimental data.

3.1 Heat Release

For a closed, adiabatic system, such as a bomb calorimeter, the heat released by the reaction would be captured entirely by the solid sample and could be calculated simply by:

$$Q_{reaction} = Q_{solid} \tag{3}$$

However, our experimental setup is an open, non-adiabatic system. In this case, the heat released by the reaction will be absorbed by the solid, absorbed by the gas flowing through the solid, or lost to the surroundings. It can be calculated by:

$$Q_{reaction} = Q_{solid} + Q_{gas} + Q_{surroundings} \tag{4}$$

Fortunately, each of the terms on the right hand side of this equation can be determined through the temperature and flow measurements, as explained next.

One assumption used in this method is that the reaction begins when an increase in the temperature is first noticed, and finishes when the peak temperature is reached. In fact, the reaction will still be occurring when the peak temperature is reached, but the heat absorbed by the flowing gas and the surroundings will be greater than that produced by the reaction, causing the observed temperature to peak then drop. Unfortunately the design of the experiment does not allow a determination of the time the reaction actually stops. The result of this assumption is that the calculated heat release will be less than the actual heat release. This is estimated to result in an error of about 10% of the total based on detailed examination of one of the data sets.

Firstly, the heat lost to the surroundings, $Q_{surroundings}$, was found to be less than 0.01% of the total, so it is ignored in analysis of the data. However, the method for estimating it is shown in Appendix A for reference.

To calculate the heat absorbed by the solid and gas, the sample volume is divided into four parts consistent with the placement of the four thermocouples, as shown in Figure 9. In this way, the thermocouple reading is used to represent the average temperature of its respective region. The area of each region is multiplied by the sample depth (measured for each run) to provide its respective volume.

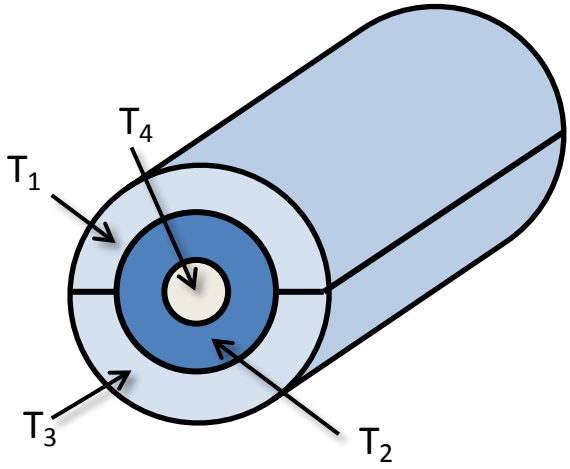

Figure 9: Division of the sample volume into four parts, each ones average temperature represented by the thermocouple reading shown (T_1 to T_4).

The total heat absorbed by the solid, Q_{solid}, is then the sum for each region *i*:

$$Q_{solid} = \sum_{i=1}^{4} Q_{solid,i} \tag{5}$$

The heat absorbed by the solid in each region *i* is calculated by:

$$Q_{solid,i} = V_i \rho C_{p,solid} \left(T_{peak,i} - T_{initial,i}\right) \tag{6}$$

Here, V_i represents the volume of region *i*, ρ is the density of the sample (calculated from its measured mass and overall volume for each run), and $C_{p,solid}$ is the specific heat of the sample. $T_{peak,i}$ is the maximum temperature reached in region *i* during the oxidation, while $T_{initial,i}$ is the temperature just before the oxidant reacts with the sample.

Density is calculated for each run simply based on the measured amount of material and total volume. The specific heat depends on the material being tested: what, if any, inactive material is present and in what amount. Table 1 lists the specific heat values used for each material considered. When a mixture was tested a mass average was used to calculate the specific heat of the bulk sample.

Table 1: Values of specific heat used for each material.

Material	Specific Heat (kJ/kg-K)	Condition	Ref.
Active material	1.047	Room temperature	[17]
Polystyrene	2	200 °C	[19, 20]
Siloxane	1.625	350 K	[21]

The heat absorbed by the gas flowing through the sample (Q_{gas}) was also calculated on a per-region basis according to:

$$Q_{gas} = \sum_{i=1}^{4} Q_{gas,i} \tag{7}$$

With the heat absorbed by the gas in each region calculated by:

$$Q_{gas,i} = \sum_{t_{initial}}^{t@T_{peak,i}} \frac{A_i}{A_{total}} \dot{m} C_{p,gas} \left(T_{t,i} - T_{gas,inlet}\right) \Delta t \tag{8}$$

Where A_i represents the cross-sectional area of region *i*, A_{total} is the cross-sectional area of the vessel, $\dot{m}$ is the mass flow rate of the flowing gas, and $C_{p,gas}$ is the specific heat of the gas. $T_{t,i}$ is the temperature reached in region *i* during the oxidation at some time *t*, while $T_{gas,inlet}$ is the temperature of the oxidant at the vessel inlet (i.e., room temperature). The equation is calculated for each measurement time interval, represented by Δt, and summed starting from the time the reaction first begins ($t_{initial}$) to the time the peak temperature is reached ($t@T_{peak,i}$) to calculate the cumulative amount of heat absorbed by the gas during the exothermic phase of the reaction.

Oxidant gas specific heat is calculated using a mass average. Using room-temperature values of 1.04 kJ/kg-K for N_2, 0.9191 kJ/kg-K for O_2, and 5.19 kJ/kg-K for He and mass fractions of 0.730 for N_2, 0.269 for O_2, and 0.001 for He gives a mixture-averaged specific heat of 1.013 kJ/kg-K.

3.2 Hydrogen Capacity

Hydrogen capacity is determined by desorbing H_2 from the fully-charged (full of H_2) sample into a known, closed volume initially at vacuum (Sievert method). To understand how this is accomplished it is useful to review the details of the experimental procedure, and to assist with this a portion of the schematic from Figure 7 is shown here as Figure 10. Just prior to desorption, the region of the experimental setup between Valves 2, 3, and 5, which is called the Sample Volume, is full of H_2 gas at high pressure, and the sample is fully adsorbed with H_2. The region between Valves 3 and 4, called the Desorption Volume, is at vacuum. At the beginning of desorption, Valve 3 is opened. At this instant, the gas from the Sample Volume flows into the Desorption Volume and the pressure in the two volumes equilibrates, and is measured as P_{desorp}. The pressure and temperature of both the Desorption Volume and Sample Volume are now used to calculate the mass of gas-phase H_2 gas existing in both volumes (m_{H2}). Because the pressure is low, the ideal gas equation is used:

$$m_{H_2} = \frac{MW_{H_2}}{1000R} P_{desorp} \left(\frac{V_{desorp}}{T_{desorp}} + \frac{V_{sample}}{T_{sample}}\right) \tag{9}$$

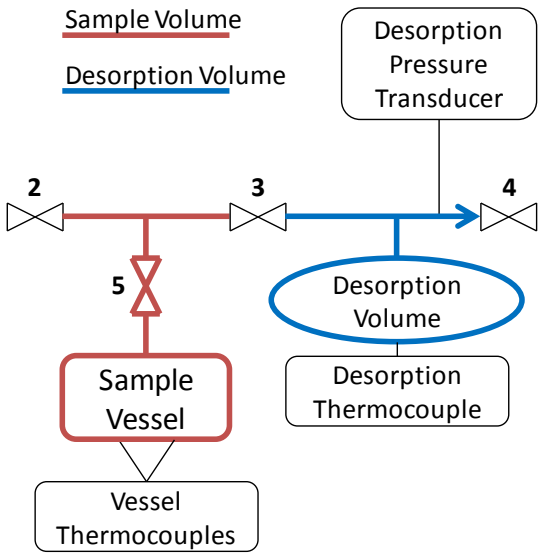

Figure 10: Detail of the experimental setup identifying the Sample Volume (red lines) and Desorption Volume (blue lines) regions.

In this equation, m_{H2} will give units of [g] when R is 0.08314 L-bar/mol-K, MW_{H2} is the molecular weight of hydrogen (2.016 g/mol), *P* has units of [bar], *V* of [cm^3], *T* of [K], and 1000 is a conversion factor from cm^3 to L.

Just after Valve 3 is opened, it is assumed that no significant H_2 is desorbed in this instant because the time is very short. Therefore, the first data point after this event is used to calculate the initial mass of H_2 gas in the volumes ($m_{H2}|_{t0}$) using Eq. (9). The amount of H2 desorbed at any time *t* is then:

$$m_{H_2,desorp} = m_{H_2}\big|_t - m_{H_2}\big|_{t0} \tag{10}$$

The equation used to calculate the weight percent of hydrogen that the material stored is:

$$wt\% = \frac{m_{H_2,desorp}}{m_{metal\ hydride}} \tag{11}$$

By choosing the mass of the metal hydride as the denominator in Eq. (11) rather than the sample mass, comparisons of capacity between the different materials can be made on the same basis regardless of the amount of polymer present. This method is essential because the different composite blends have different polymer contents due to variations during synthesis.

Although the capacity values are calculated for every time step during a single desorption cycle, just the last data point is used to give the total amount of hydrogen desorbed during the cycle.

Because there is a slight (< 5 second) delay between the opening of Valve 3 and the recording of the first data point, the calculated initial value may be slightly too large. The result of this is that the calculated weight percent may slightly under-predict the actual weight percent.

Another possible way to calculate the initial mass is to find the mass within the Sample Volume just *prior* to Valve 3 opening. Because the gas in this state is at high pressure, this can be done with a non-ideal gas equation of state, such as van der Waal's equation. However, the temperature of the Sample Volume is not measured directly and using the sample vessel temperature as a substitute will surely be too high of an estimate because the bulk of the Sample Volume is tubing that is not heated. Although the same is true when the Desorption Volume method is used, the Sample Volume (11.7 cm^3) is small in proportion to the Desorption Volume (1,974 cm^3) so the resulting error is much smaller (negligible).

3.3 Durability

The durability of the additive is defined as its ability to mitigate the hazardous reaction after it has been "used" (i.e., tested in realistic operating conditions). There is no specific test for durability; rather the results from several experiments are used to determine durability.

A sample that is cycled many times is then oxidized using the flow-through calorimeter, and the heat release is compared to a sample of the same material that has not undergone cycling. If the heat release after cycling has increased, the material is not mitigating as it did before and is one indication that it is breaking down. The additive content of the sample is also measured before and after cycling using TGA. If the amount of polymer present after cycling is less than it was before, this is another indication that the additive is breaking down. Combined, these three tests are used to determine the additive's durability.

4 Results and Discussion

4.1 Composite Synthesis and Characterization

Synthesis of composite materials: Our target weight percent of polymer relative to the total composite mass was 10 – 20 weight percent (wt%). Lower values are better from an efficiency point-of-view but may not mitigate effectively. Initial experiments focused on finding conditions in which styrene (St) and divinyl benzene (DVB) could be polymerized in the presence of metal hydrides to give a composite material containing nearly 20 wt% polymer. Small-scale reactions were performed in 4-mL vials using various amounts of styrene, divinyl benzene, AIBN, solvent and $NaAlH_4$. From these experiments it was found that vinyl arenes could be polymerized under free-radical polymerization conditions to furnish cross-linked networks in the presence of sodium alanate. Yields for the polymer portion of the composite were slightly lower than neat polymer yields but typically approached 85%.

As shown in Figure 11, the thermal decomposition of the composite materials starts above 250 °C and continues to 400 °C. For this 3:4 St/DVB composite material a 6.2 wt% loss was observed. The calculated polymer wt% in the composite material was 13.5 wt% based on the mass yield. For comparison, the neat polymer TGA trace is shown in red which shows the onset temperature is shifted higher, to around 370 °C, with an overall wt% loss of 73.1% (Note that comparing wt % loss numbers between the composite and neat materials is not meaningful because of the different fractions of polymer in the two materials.)

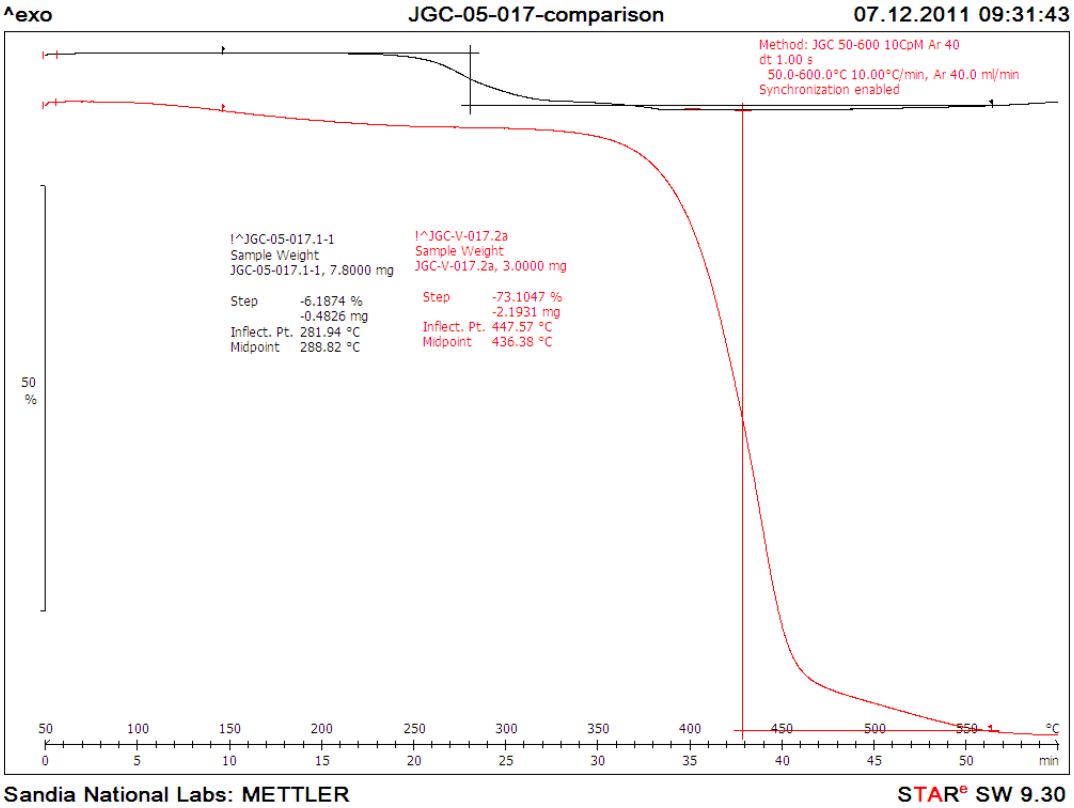

Figure 11: TGA of 3:4 St/DVB composite material (black trace) showing decomposition onset temperature of approximately 250 °C compared to neat polystyrene (red trace) at approximately 370 °C. Y-axis is not to scale.

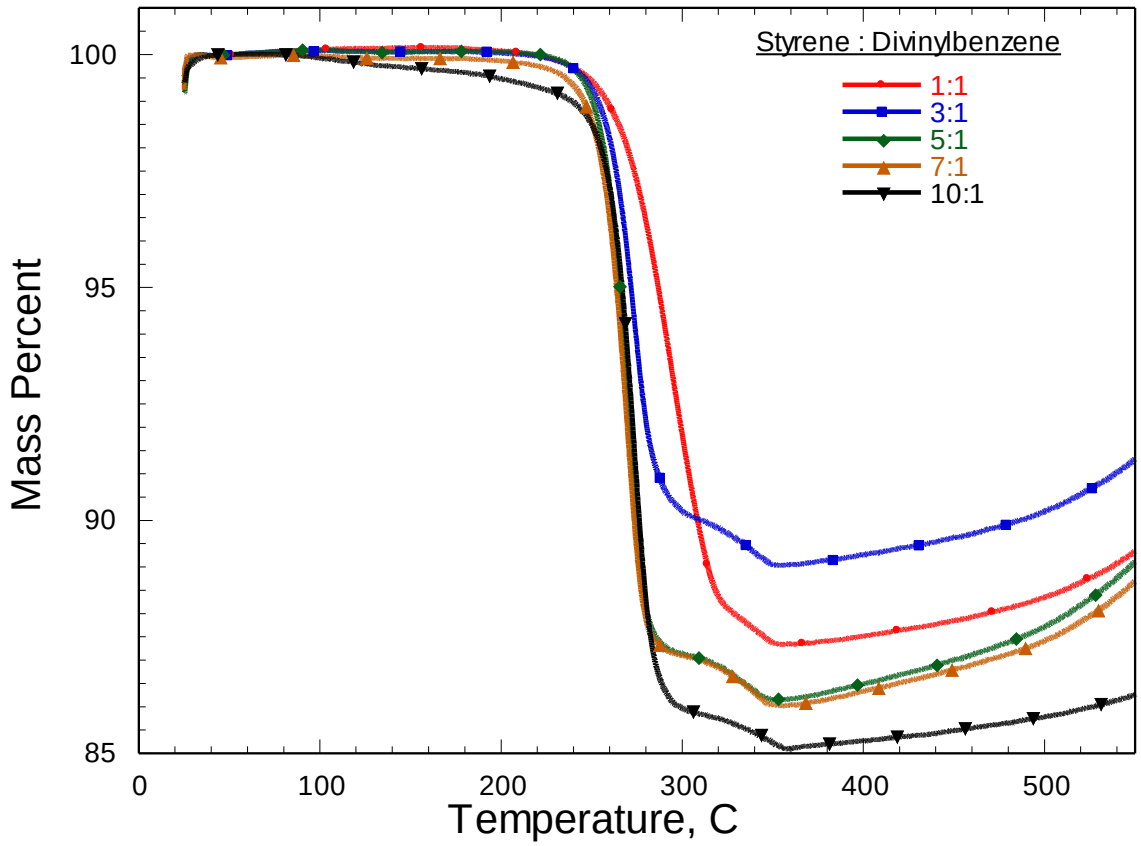

Figure 12: TGA comparisons of different cross-linked polystyrene composite polymers.

Consistent with previous work it was found that higher St/DVB ratios gave harder/tougher materials compared to more brittle composite materials that formed from lower St/DVB ratios. It is hypothesized that when more DVB is added, the amount of cross-linking increases causing a more brittle network compared to one that has a lower cross-linking density. The preferable outcome is a more brittle material since it is easier to crush and handle compared to a hard/tough composite material. While the physical properties of the material varied with cross-linking density, the thermophysical properties as measured by TGA were largely independent of cross-linking density. Figure 12 shows TGA traces of composite materials with different St/DVB ratios. All materials, regardless of cross-linking density had a similar onset temperature. Small differences in the total mass loss could be attributed to different yields of char, however, they could also be attributed to different polymer wt% in the original composite material.

Since cycling to release and re-charge hydrogen gas occurs between 120 – 180 °C in the metal hydride, we cycled neat polymer material in the TGA instrument between 145 – 190 °C to determine its robustness under cycling. Figure 13 shows the TGA trace as a function of temperature for a 1:1 St/DVB polymer cycled six times between 145 and 190 °C.

The initial 3.5 wt% loss is attributed to residual solvent. After a subsequent six cycles the neat polymer loses approximately an additional 1 wt%, which is attributed to the polymer degradation, meaning

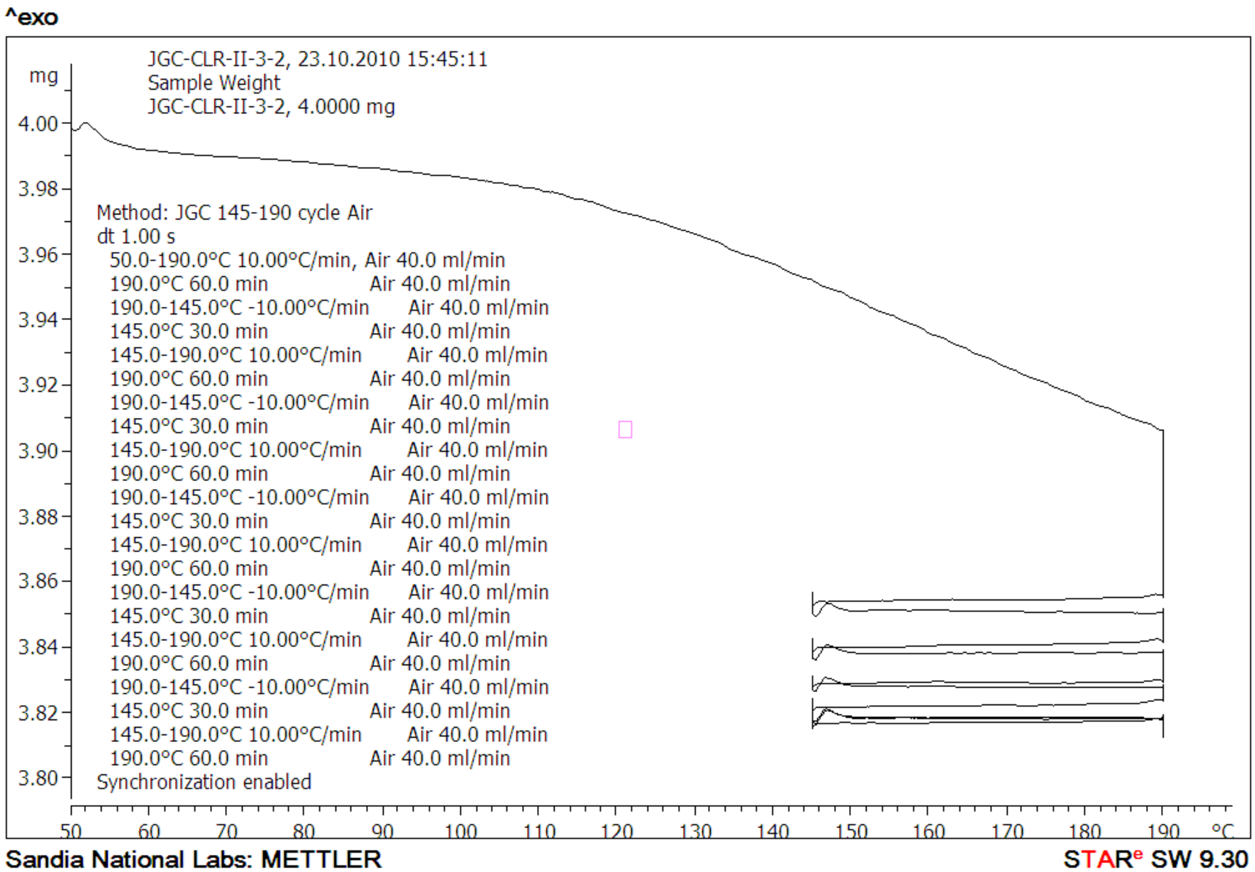

Figure 13: TGA cycling experiment between 145 - 190 °C in air of 40:1 St/DVB polymer.

nearly 99 wt% of the polymer remains after cycling in air. This result implies that a composite material cycled below 190 °C will not loose a significant amount of polymer if there are no changes in the chemical behavior of the polymer in the composite compared to the neat polymer.

SEM data: Further characterization of a polystyrene metal hydride composite material (3:4 St/DVB) was done by scanning electron microscopy (SEM). An energy dispersive spectrum (EDS) was simultaneously collected to distinguish between the phases of material (Figure 14). The inorganic portion was identified in Spectrum 1 (left picture) by the strong Na, Al and O signals. The peak for oxygen observed in the EDS is due to preparing samples in air, which rapidly oxidizes the metal hydride. On the right side of Figure 14, Spectrum 2 identifies the polymer surrounding the inorganic material by the absence of Na and Al signals and the shoulder at low energy for C.

Later, the sputter-coating of samples with gold inside a glove box was attempted. These samples were transferred to the SEM using a custom-made chamber to prevent air contamination. The best images for virgin metal hydride, composite material, oxidized material, and cycled material are shown at various magnifications in Figure 15. It is not conclusive, but the larger flake-like materials in each image are likely polymer or graphite. Further characterization is required. From these SEM experiments, the Au sputter-coated thickness and electron voltage were optimized for this particular instrument.

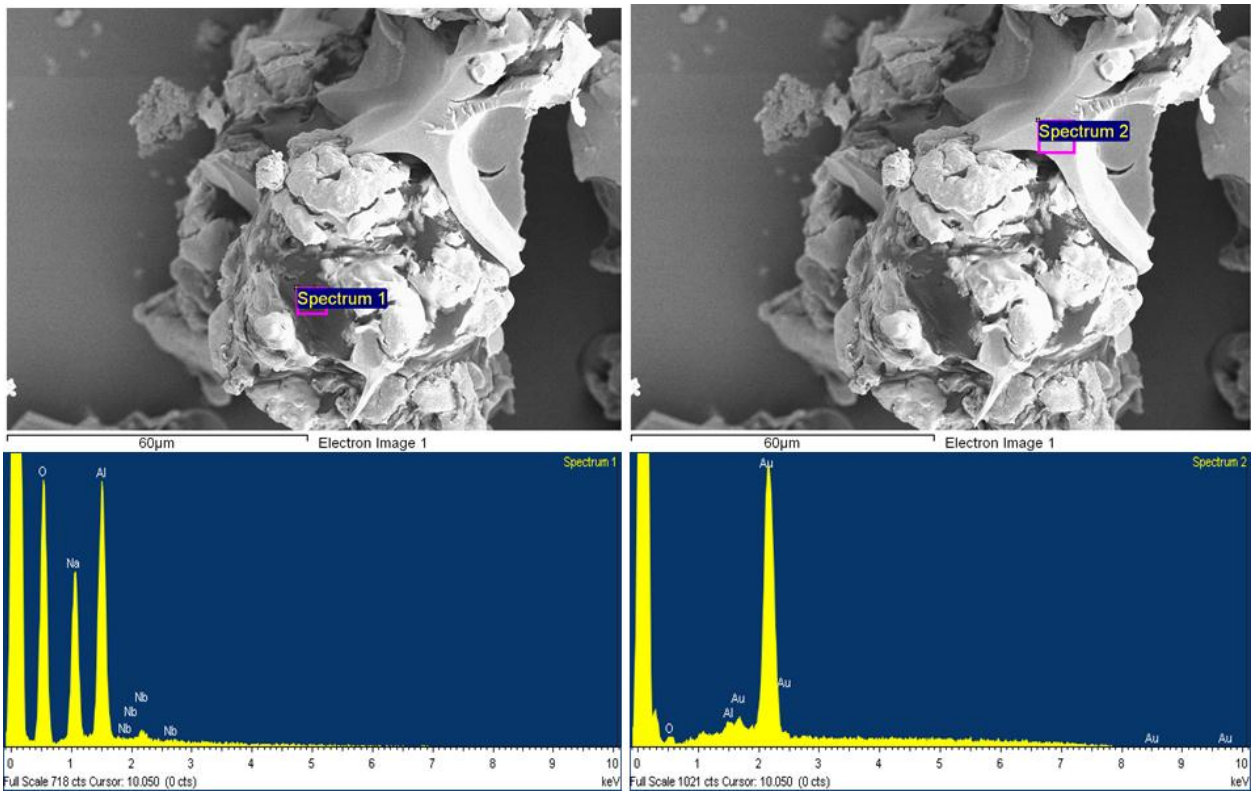

Figure 14: SEM with EDS of composite material identifying inorganic and polymer components.

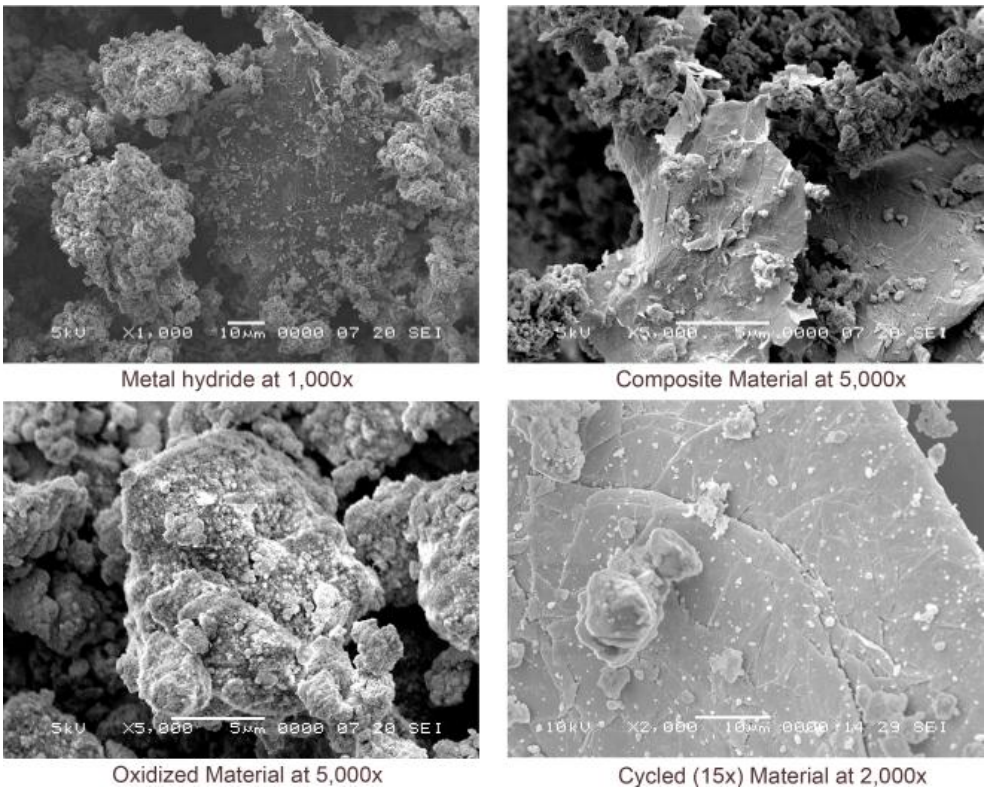

Figure 15: SEM images of material sputter-coated and kept from air.

Table 2: Characterization and properties of Siloxanes

Property/ Name	DMS-V52	(0.3-0.4 % Vinylmethylsiloxane) dimethylsiloxane) copolymer	VEE-005	VMM-010
ID number	1	2	3	4
Appearance	Clear viscous liquid	Clear viscous liquid	Liquid	liquid
^{1}H NMR in $CDCl_3$	only methyl signals near 0.28 ppm	multiple vinyl signals 6.2 – 5.8 ppm and methyl signals at 0.24 ppm. Ratio 1:195.0	Three sets of signals in 1:1:1.5 ratio at 6.2, 3.9 and 1.2 ppm.	Two signals with 1:1.4 ratio at 6.2 and 3.5 ppm.
Toluene Solubility	soluble	soluble	soluble	soluble

Siloxane Composite Materials: It is well known that siloxane (-R_2SiO-) based polymers are elastomeric polymers with high char-forming properties upon thermolysis. Attempts to find a suitable siloxane-based monomer that could be polymerized in the presence of a reactive metal hydride were difficult. Most vinyl containing siloxanes require the use of a platinum or palladium catalysts for polymerization. However, a few monomers were identified from Gelest, Inc. which contain vinyl siloxanes—a functional group susceptible to free-radical polymerization. Table 2 summarizes the siloxane purchased from Gelest, Inc. for this work and some of their physical properties.

Initial experiments were performed to determine whether various combination of the siloxanes could be polymerized using AIBN as an initiator in toluene. Ten different combinations using approximately 1:1 mass ratios of two siloxanes dissolved in a toluene solution containing AIBN to initiate polymerization (Table 3) were prepared. Of these ten combinations, only three gave solid materials. The other seven

Table 3: Polymerization of siloxanes with AIBN in toluene.

Reaction Number	Mass (g) of siloxane by ID number (Table 2)				% Yield	Appearance
	1	2	3	4		
1	0.5897	0.6473	0	0	97.8	Liquid
2	0.4213	0	0.4283	0	22.6	Liquid
3	0.5243	0	0	0.5049	89.1	White Paste
4	0.5066	0	0	0	98.0	Liquid
5	0	0.4727	0.4953	0	86.8	White Paste
6	0	0.4254	0	0.4892	83.5	White Paste
7	0	0	0.5557	0.477	84.1	Solid
8	0	0	0.6091	0	76.4	Solid
9	0	0	0	0.6974	81.0	Solid
10	0	0.5862	0	0	98.0	Liquid

Table 4: Siloxane composite materials.

Reaction Number	Mass (g) M-H	Siloxane ID number	Theoretical yield[(a)]	Dried Mass (g)	% Yield	Theor. Polymer Yield	Actual polymer yield	% Polymer Yield
11	3.3791	**3**	4.133	3.8076	92.12	0.7543	0.4285	56.81
12	3.1965	**4**	3.899	3.6398	93.35	0.7026	0.4433	63.09
13	3.1025	**3** and **4**	3.853	3.5258	91.51	0.7503	0.4233	56.42
14	0	**3**	1.073	0.9125	85.01	1.0734	0.9125	85.01
15	0	**4**	1.051	0.7183	68.33	1.0512	0.7183	68.33
16	0	**3** and **4**	1.110	0.9522	85.75	1.1104	0.9522	85.75

[a] Theoretical yield assumes AIBN decomposes to lose N_2 with a 17% loss in mass

gave liquids or paste-like materials with no evidence of polymerization. The lack of polymerization for **1** and **2** is not surprising due to the low concentration of vinyl groups compared to methyl groups as determined by ^{1}H NMR spectroscopy. Based on these preliminary results, siloxanes **3** and **4** were chosen to make composite materials with sodium alanate.

Three stock solutions containing siloxanes, toluene, and AIBN were prepared with the aim of having 10 – 20 wt% siloxanes relative to metal hydride upon polymerization. The stock solutions were made in approximately the same concentrations as reaction numbers 7, 8, and 9 in Table 3. The stock solutions were added to the prepared metal hydride in 8 mL reaction vials. Polymerizations were performed as with St/DVB mixtures discussed above. Table 4 summarizes the results, including the polymer yield within the composite materials. Portions of the stock solutions (reaction numbers 14, 15, and 16) were also polymerized without metal hydride to get a direct comparison of the yield and physical properties.

The polymerization reactions of the stock solutions containing only siloxanes (reactions 14-16) had polymer yields similar to those seen in Table 3 for mixtures of **3** and **4** (reactions 7-9). Interestingly, the corresponding polymer yields calculated for the composite materials were significantly lower (reactions 11-13). Therefore, the actual polymer weight percent in the composite material was closer to 12% rather than the desired 20 wt%.

TGA/DSC coupled to a mass spectrometer was used to characterize the thermal decomposition of the six samples made in Table 4. As seen by TGA, the decomposition temperature of the cross-linked polystyrene composite materials is significantly perturbed compared to the pure siloxanes polymer. Figure 16 and Figure 17 show representative TGA/DSC-MS traces of materials from reactions 13 (with

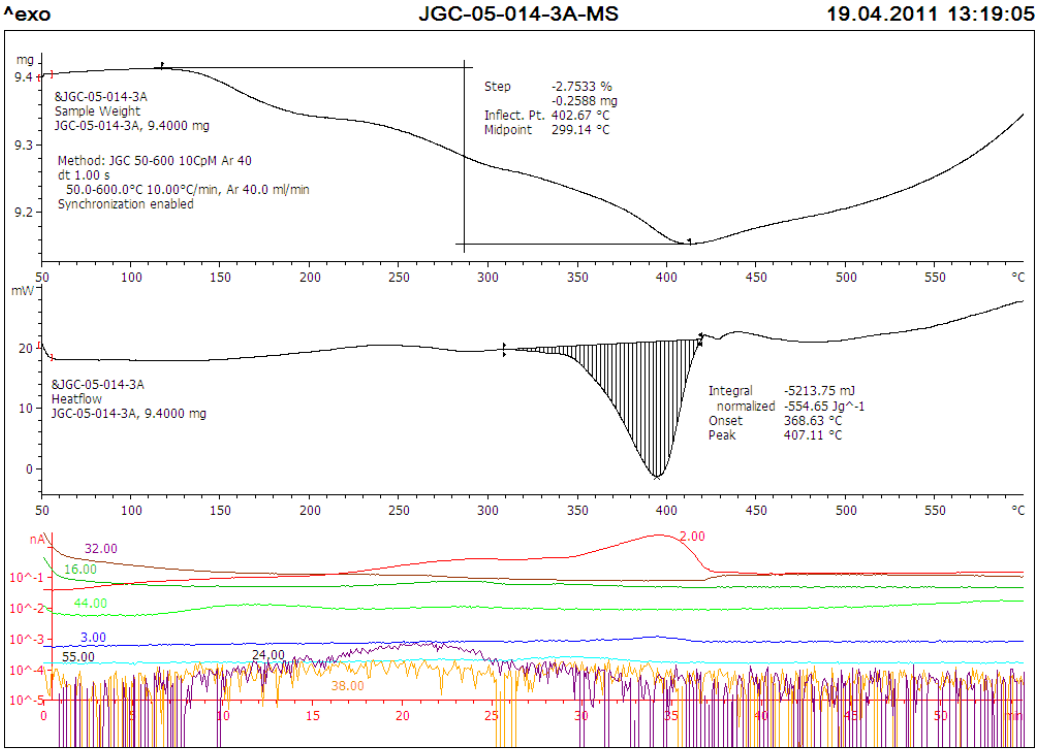

Figure 16: TGA/DSC-MS trace of siloxane composite material containing 3 and 4.

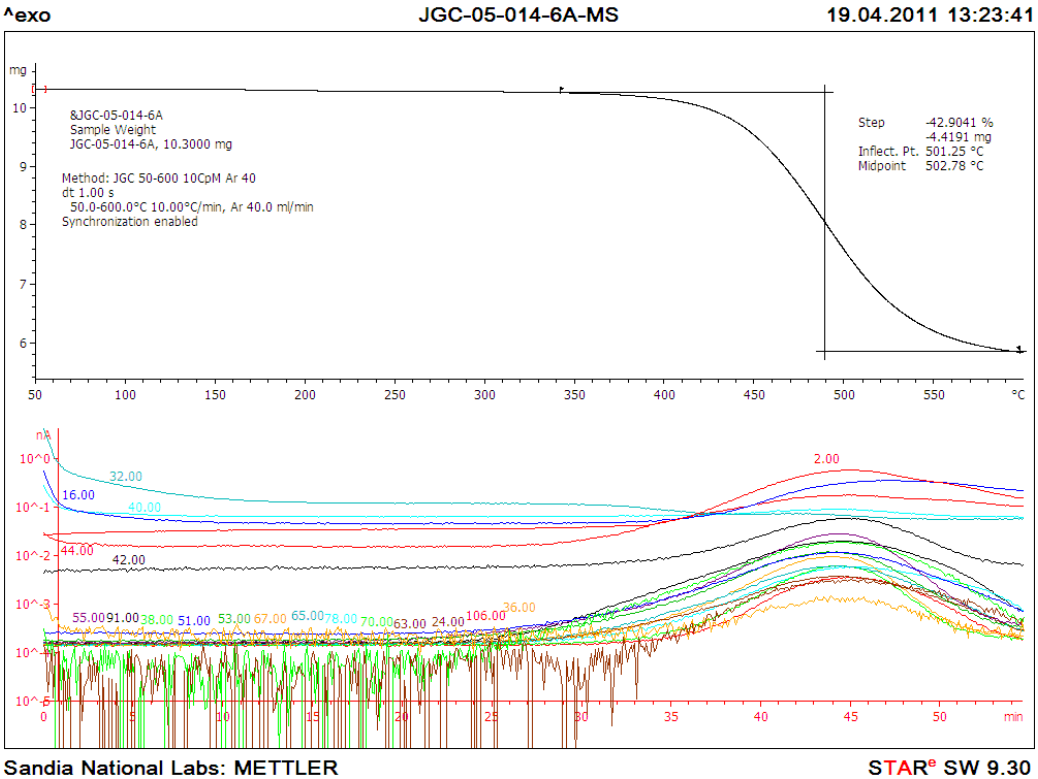

Figure 17: TGA/DSC-MS trace of siloxane polymer containing 3 and 4 with no metal hydride.

M-H) and 16 (without M-H), respectively. (The high signal-to-noise seen in the bottom MS trace is due to a short dwell time on a very low-abundant ion.)

The differences between the thermal decomposition pathways are striking. Neat (no M-H) siloxanes polymer based on **3** and **4** (Figure 17) has an onset temperature above 370 °C (DSC data was not included for clarity) and loses 42 wt%. This means, nearly 58 wt% of the original polymer remains as a char-forming material. In contrast, Figure 16 shows that when siloxanes **3** and **4** are polymerized in the presence of the M-H, the thermal decomposition begins as low as 100 °C. Based on the polymer wt% yields in Table 4 and the TGA/DSC data collected for reactions 11-16, it appears that composite materials with only siloxanes present are unsuitable for hazard mitigation application. This conclusion is unfortunate since the neat siloxanes polymer itself has a high char-formation compared to cross-linked polystyrenes. Of the three composite materials mentioned above, reaction 12 was used for preliminary cycling studies because it had the highest thermal stability.

Hypothesizing that the vinyl density in the siloxanes is too low to adequately cross-link the polymer network in the presence of metal hydride, we explored the possibility of adding styrene and/or divinyl benzene to the mixtures. In a similar fashion to the above experiments, 18 unique reaction mixtures were heated to determine if solid polymers formed. Of the 18 mixtures, only five gave solid materials after completely drying. The yields of these five solids ranged between 104 – 93% (possibly due to residual solvent trapped in the polymer). These five samples were analyzed by TGA/DSC-MS to determine the thermal degradation properties. A small mass loss near 100 °C with an exothermic heat flow, followed by a large mass loss above 370 °C is observed for all five samples. It is unclear to what the first mass-loss is attributed. The latter mass loss near 370 °C is most likely due to decomposition of the siloxane/styrene-based polymer. Figure 18 is representative of the thermal decomposition trace for a 1:1 mixture of styrene and siloxanes **4** as measured by TGA/DSC. The total mass loss, shown on the top curve, is 61.1 wt%. This mass loss is approximately 20% higher than a polymer made only with siloxanes **4**, likely due to the presence of styrene which does not form char. Some char formation is evident since 39 wt% of polymer remains even up to 550 °C.

A composite material was made using styrene, divinyl benzene, and siloxanes **4** in approximately 4:1:4 ratio by mass with the aim of a 20 wt% polymer composite product. The resulting solid was a hard mass that was not easily broken or crushed. The polymer yield, as determined by mass was 66.1%, which meant that the final composite material contained 13.7 wt% polymer. A solution containing only monomers was simultaneously polymerized to give a hard opaque solid. The yield of this neat polymer was 104.2%, which can only be attributed to residual solvent in the sample. Both samples were analyzed by TGA/DSC. Figure 19 shows the TGA/DSC of the neat polymer, run twice for repeatability. The upper TGA trace shows a reproducible midpoint temperature for the thermal decomposition near 440 °C. The total weight loss is approximately 70%.

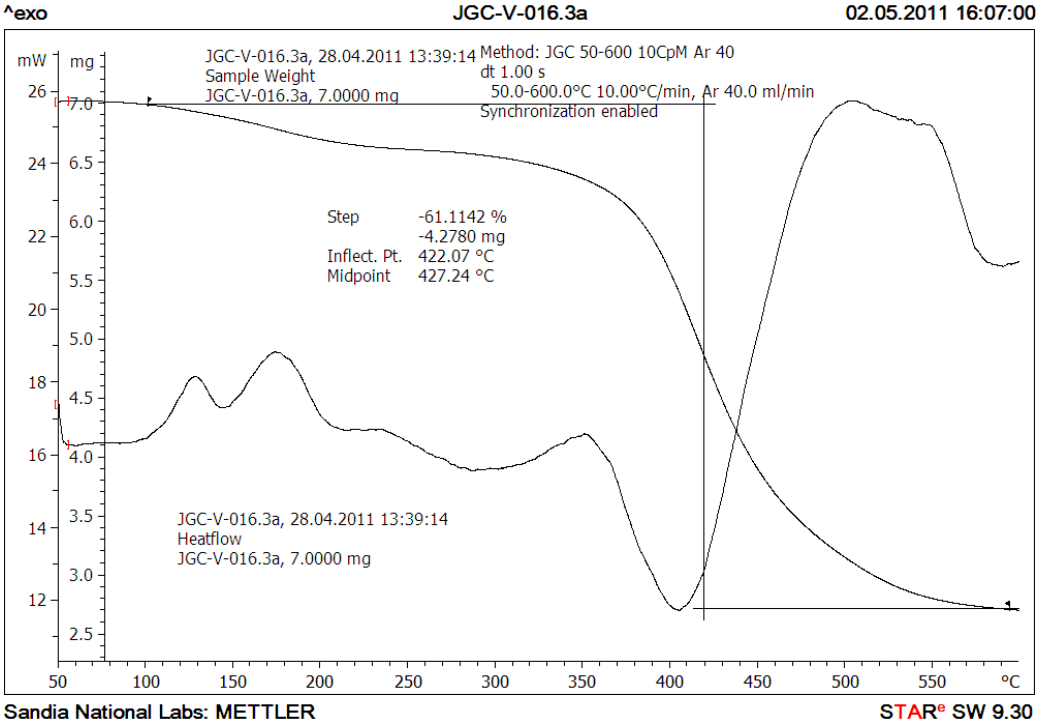

Figure 18: TGA/DSC of neat polymer made from styrene and siloxane 4 in 1:1 mass ratio. Top curve is TGA and bottom curve is DSC trace.

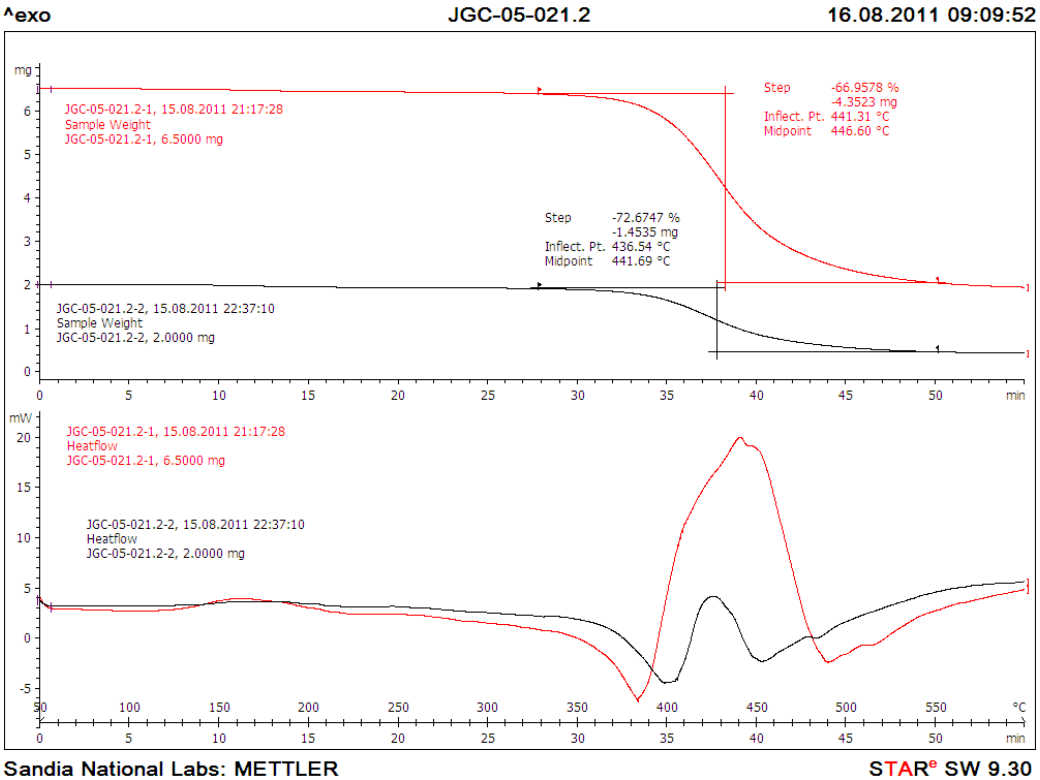

Figure 19: TGA (upper) and DSC (lower) traces of 4:1:4 St/DVB/Siloxane neat polymer in argon (showing duplicate runs).

In contrast, the composite material made from the same monomer formulation shows a thermal degradation with a midpoint at 309 °C (Figure 20). Interestingly, the DSC shows an endothermic heat-flow, whereas the neat polymer degrades exothermically. Clearly, the chemical nature of the polymer is significantly perturbed in the composite. However, since the thermal degradation of this composite material is substantially higher than the cycling temperature of the metal hydride, and it does give char upon decomposition, this material was selected for further analysis.

These siloxane materials were also analyzed by TGA/DSC-MS after cycling, with the results shown in Figure 21 for siloxane composite material made with 1:1:0.5 **4**:St:DVB. Samples were taken after one and 30 hydrogen-sorption cycles. As seen in the figure, very little change in the wt% loss could be detected after 1 (green curve) or 30 cycles (red curve) compared to the uncycled composite material (blue curve), with all three samples losing approximately 4.2 to 4.5 wt%, even after 30 cycles. The accompanying DSC and MS data (not shown) also do not reveal any significant differences between the three samples.

These preliminary results are encouraging because with additional cycles, the siloxane composite material has nearly the same wt% loss as measured by TGA and the onset temperature for thermal decomposition is slightly higher than the all-polystyrene composite material (as was seen by comparing Figure 11 and Figure 12 with Figure 20).

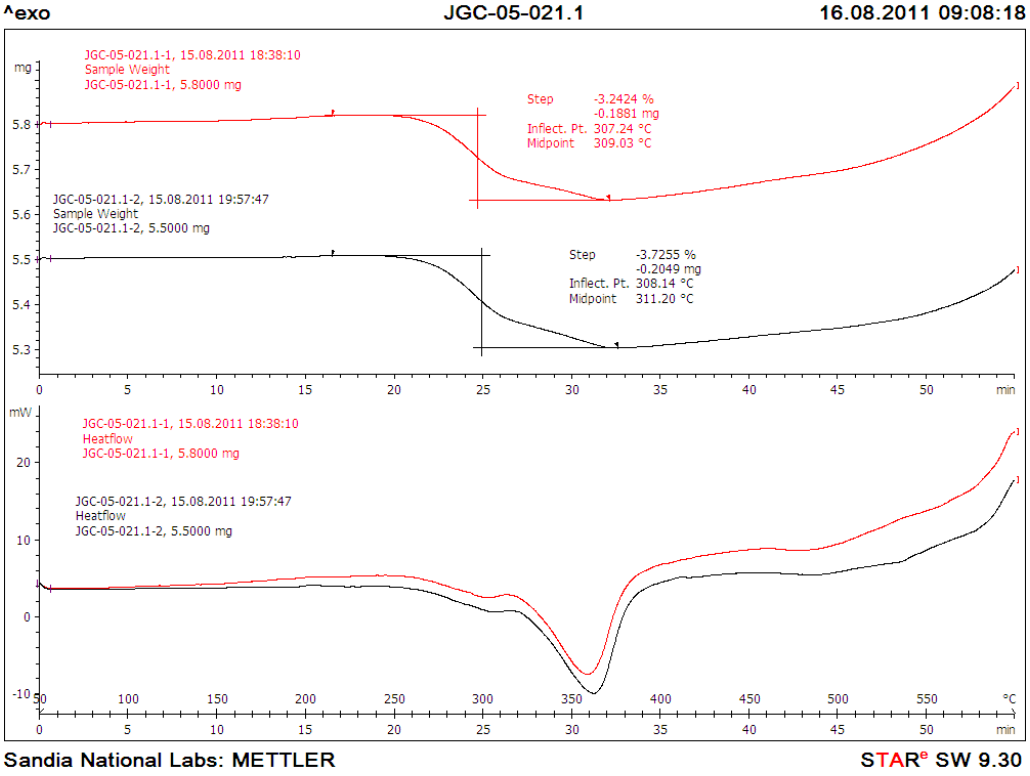

Figure 20: TGA (upper) and DSC (lower) traces of 4:1:4 St/DVB/Siloxane composite material in argon (showing duplicate runs). Total polymer composition is 13.7 wt% of solid.

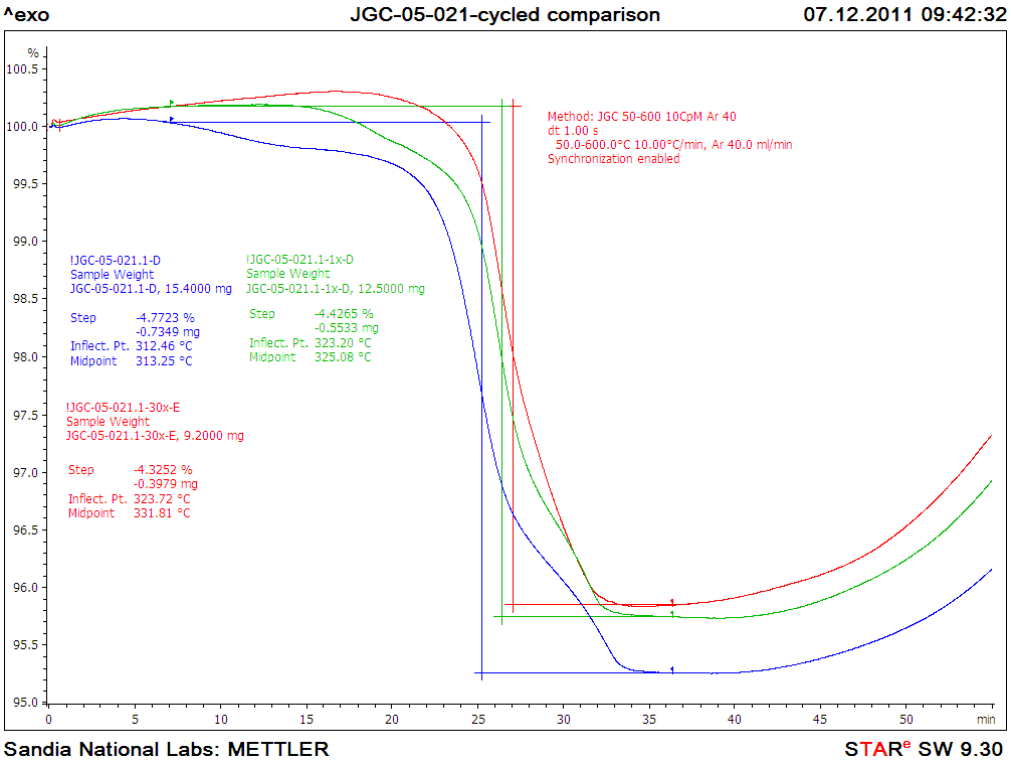

Figure 21: TGA traces of neat (blue), 1x hydrogen-soption (green), and 30x hydrogen-soption (red) siloxane/polystyrene composite materials made with 1:1:0.5 4:St:DVB.

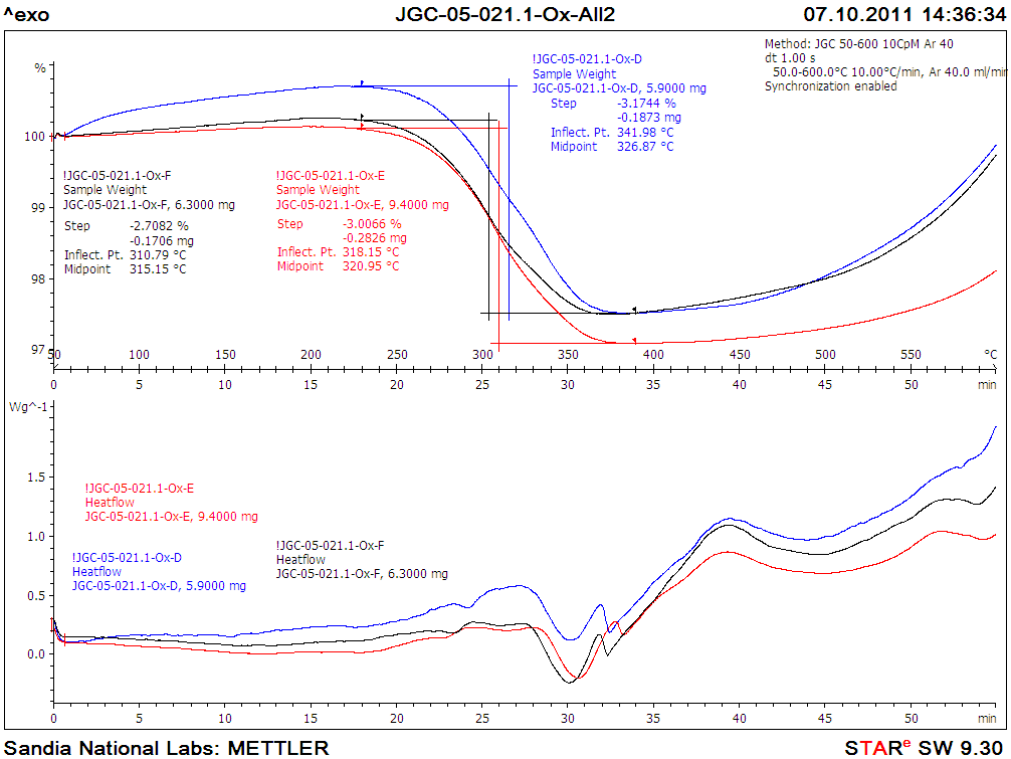

Figure 22: TGA/DSC trace of oxidized siloxane-PS composite material repeated three times.

An oxidized sample was analyzed by TGA/DSC-MS and the results are shown in Figure 22. This oxidized uncycled composite material shows a modest weight loss that is statistically lower at 3 wt% than any of the siloxane composite material tests shown in Figure 21. Compared to the over 4 wt% mass loss of the uncycled material, this indicates that, during oxidation, more than three-fourths of the polymer was converted to a stable form (char) during oxidation, as intended. The shape of the TGA curve is also slightly different than that observed for the uncycled composite material. The DSC trace is most perturbed from the uncycled composite material with both endothermic and exothermic heat flows beginning near 300 °C, continuing to 450 °C.

4.2 Hydrogen Capacity

Figure 23 shows the dependence of hydrogen capacity on the type of mitigating material and number of cycles up to 30. From this figure it can be seen that the addition of the polymer decreases the hydrogen capacity compared to the unmitigated, neat material. Because the capacity is calculated on a per-weight basis of metal hydride (according to Eq. (11)), the effect shown is not because of the displacement of metal hydride with polymer, but rather a result of some change in the ability to adsorb and/or desorb hydrogen of the metal hydride itself.

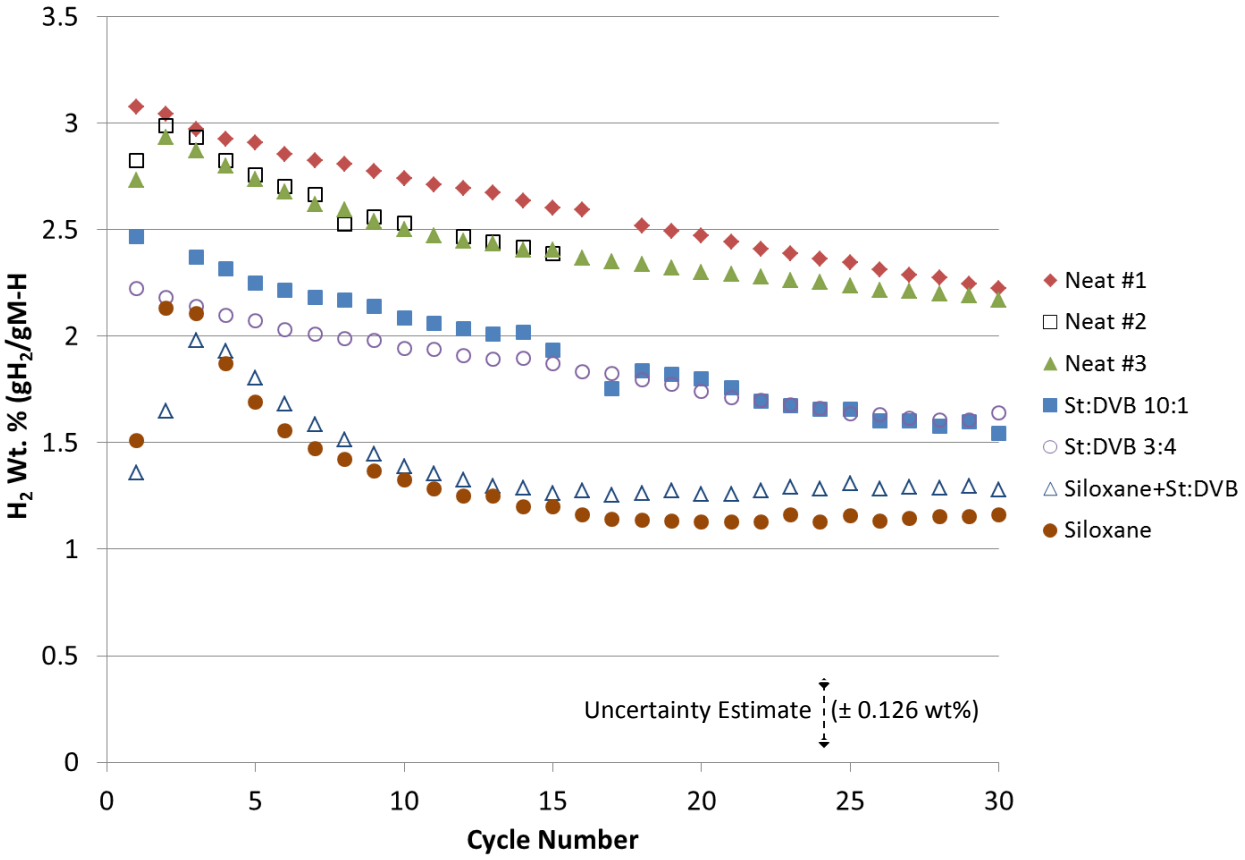

Figure 23: Capacity of the samples as a function of cycling. The capacity is calculated per gram of active material only so that all materials are evaluated to the same basis.

A few trends in Figure 23 are noticeable. One is that for two of the three neat samples, and for both of the siloxane-containing samples, the measured capacity sharply increases in the first 2-3 cycles. This could be due to an activation effect of the metal hydride, which has been observed elsewhere for sodium alanate. However, in the case of the siloxane-containing materials, it may be an artifact of the measuring process. Recall that hydrogen capacity is determined by measuring the increase of pressure in a known volume. This method assumes that the only gas evolving from the sample is hydrogen. But if the mitigating material is degassing, this will add non-hydrogen gas to the same volume and will cause the pressure to rise, and will be indicated by a larger than normal capacity. Therefore, it is possible that the large increase in measured capacity in the first few cycles of the siloxane-containing materials is a combination of both a real effect (M-H activation) and a measurement artifact (degassing of the polymer). Unfortunately, gas composition measurements were not conducted on the desorption volume so further tests would be needed to determine if this is indeed a factor.

Another trend shown in Figure 23 is regarding the slopes of the capacity measurements. For the neat material, the hydrogen capacity decreases with the number of cycles. This loss of capacity has been observed elsewhere and is attributed to morphological changes. It can also be seen that the styrene-divinylbenzene (St:DVB) materials have nearly the same degradation slope as the neat material. Thus it seems likely that the addition of the St:DVB has no effect on the inherent degradation behavior of the M-H. This is in contrast to the siloxane-containing materials, which show a large degradation from 3 to 15 cycles, but then have no degradation for the remaining 15 cycles. One possible explanation of this observation is that the siloxane in some way acts as a stabilizing agent. It is known that silica (SiO_2) can act as a carrier, support, and/or promoter for catalysis, in some cases limiting morphological changes and preserving stability of the active phase [22]. In our case, if some of the siloxane is changing to SiO_2 during the initial cycling period, it is plausible that SiO_2 has this effect on the sodium alanate reaction as well. This is only conjecture at this point, but may warrant further investigation.

Two of the tests, the low-crosslinked 10:1 styrene/divinylbenzene (St:DVB) and highly-crosslinked 3:4 St:DVB composites were cycled continuously for nearly two weeks, achieving over 180 total cycles each. The capacity measurements of these tests are shown in Figure 24. In the 10:1 test, the test was interrupted at 15 and 30 cycles to obtain TGA samples. While the impact of the 15-cycle interruption is not clear, the 30 cycle interruption produced a break in the data and showed that the material recovered some of its capacity during this time. Furthermore, the sample showed an *increasing* capacity trend from cycle 31 to about cycle 110 before beginning to degrade once more. It is postulated that the 10:1 material is decomposing more than any other mitigating material (because of its low crosslinking), and as it decomposes its tempering effect on metal hydride capacity is being diminished faster than the metal hydride degrades. According to this theory and the cycling data, around 100 cycles, the 10:1 material would be completely degraded and then natural sodium alanate degradation dominates. This is not a confirmed hypothesis but it is supported somewhat by the TGA results (Figure 25) which show a large mass loss in the first 30 cycles of the 10:1 material, and almost no change in mass loss from 30 to 180 cycles.

The 3:4 material test was also interrupted at 30, 60, and 120 cycles to obtain TGA samples. In the first two cases capacity recovery following the interruption is apparent. Unlike the 10:1 case, the 3:4 sample capacity continues to decrease as the number of cycles is increased. The polymer mass loss as a function of cycles also seems to indicate a more stable material (see Figure 25). In line with the decomposition theory stated above, the 3:4, highly-crosslinked material is more robust under cycling and continues to temper hydrogen capacity.

Note that in Figure 24 there are periodic fluctuations in the data, especially apparent in the 3:4 test after 100 cycles. These are due to diurnal changes in temperature causing the supply pressure of the hydrogen (stored outdoors) to similarly vary (one calendar day corresponds to 15-16 cycles). This in turn is slightly affecting the amount of hydrogen adsorbed by the metal hydride when exposed to this pressure.

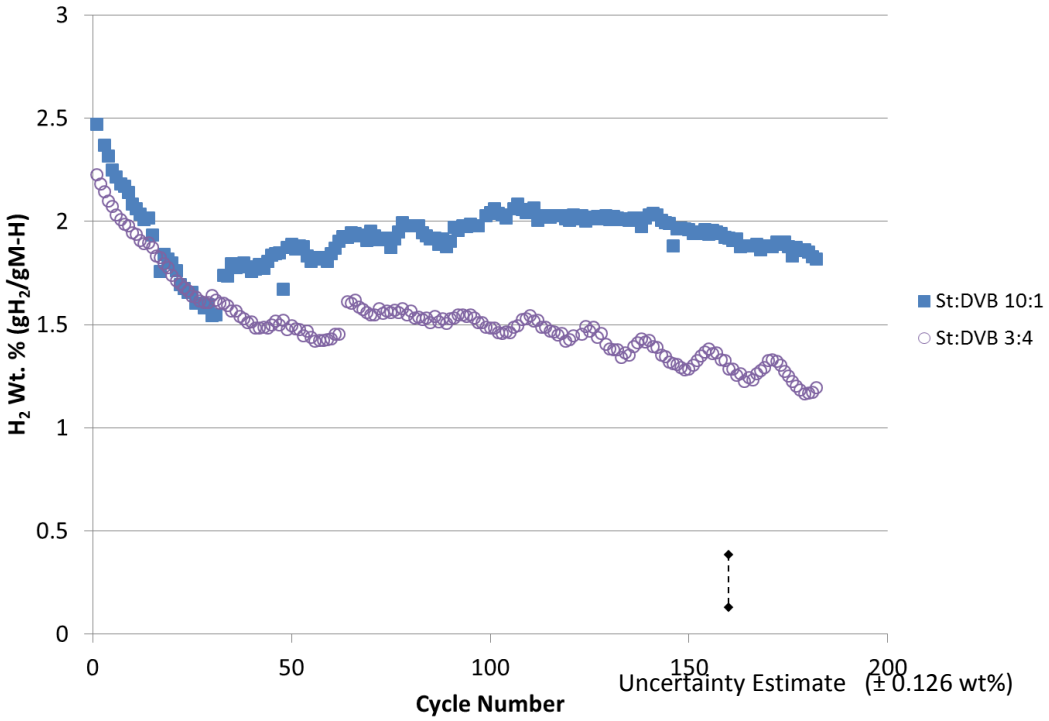

Figure 24: Long-term cycling capacity of the two styrene/divinylbenzene (St:DVB) composite materials, per gram of active material (M-H). The 10:1 test was halted and restarted after obtaining TGA samples, at 15 and 30 cycles. The 3:4 test was likewise interrupted at 30, 60, and 120 cycles. In both cases, this resulted in a recovery of lost capacity at these points. Periodic fluctuations are result of diurnal temperature changes.

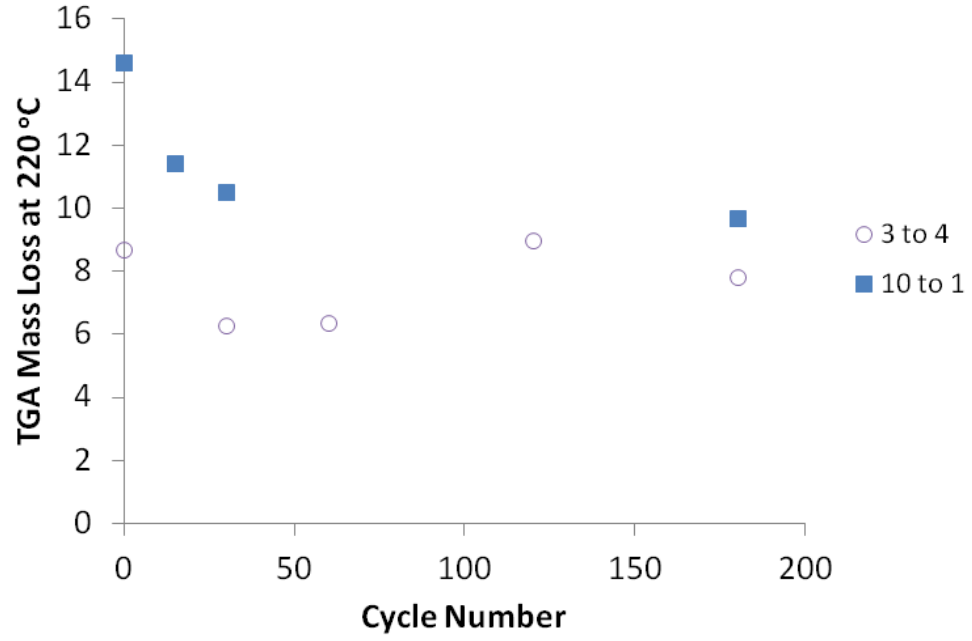

Figure 25: Mass loss of the styrene/divinylbenzene (St:DVB)-containing composite materials as a function of cycling. The 10:1 shows a large initial mass loss followed by a time of little mass loss (from 30 to 180 cycles). The data for the 3:4 material seem to indicate a mass loss that increases with increasing cycle number, indicating a more even loss of polymer throughout the test.

4.3 Heat Release

The composite materials were oxidized with the flow-through calorimeter and the amount of heat released during oxidation was calculated. Results were obtained for each polymer formulation before and after cycling, and compared to oxidation measurements for unmitigated (neat) material. A summary of the tests is given in Table 5.

Table 5: List of flow-through calorimeter tests.

Run Date	Polymer Additive	Polymer Yield (wt %)	Density (kg/m^3)	Cycles	Heat Release (J)
2009-09-23	None	0	1072	0	66.0
2009-09-29	St:DVB 3:4	15.7	991	0	40.4
2010-05-25	St:DVB 3:4	13.7	946	30	101.3
2010-08-16	None	0	957	0	76.2
2010-08-30	None	0	968	30	79.7
2011-04-28	None	0	976	1	98.0
2011-05-03	None	0	1023	1	89.4
2011-05-16	None	0	1148	1	72.0
2011-05-20	None	0	984	1	84.0
2011-06-13	Siloxane	12.2	1047	30	84.5
2011-06-23	Siloxane	12.2	1080	0	53.6
2011-07-06	Siloxane	12.0	1056	1	64.5
2011-07-13	St:DVB 3:4	13.5	964	1	92.1
2011-07-19	St:DVB 3:4	13.5	1249	1	77.7
2011-08-12	None	0	904	1	81.8
2011-08-18	Siloxane+St:DVB 2:1	14.8	1064	0	34.9
2011-08-30	Siloxane+St:DVB 2:1	14.8	1061	1	77.9
2011-09-06	Siloxane+St:DVB 2:1	14.8	1056	30	93.2

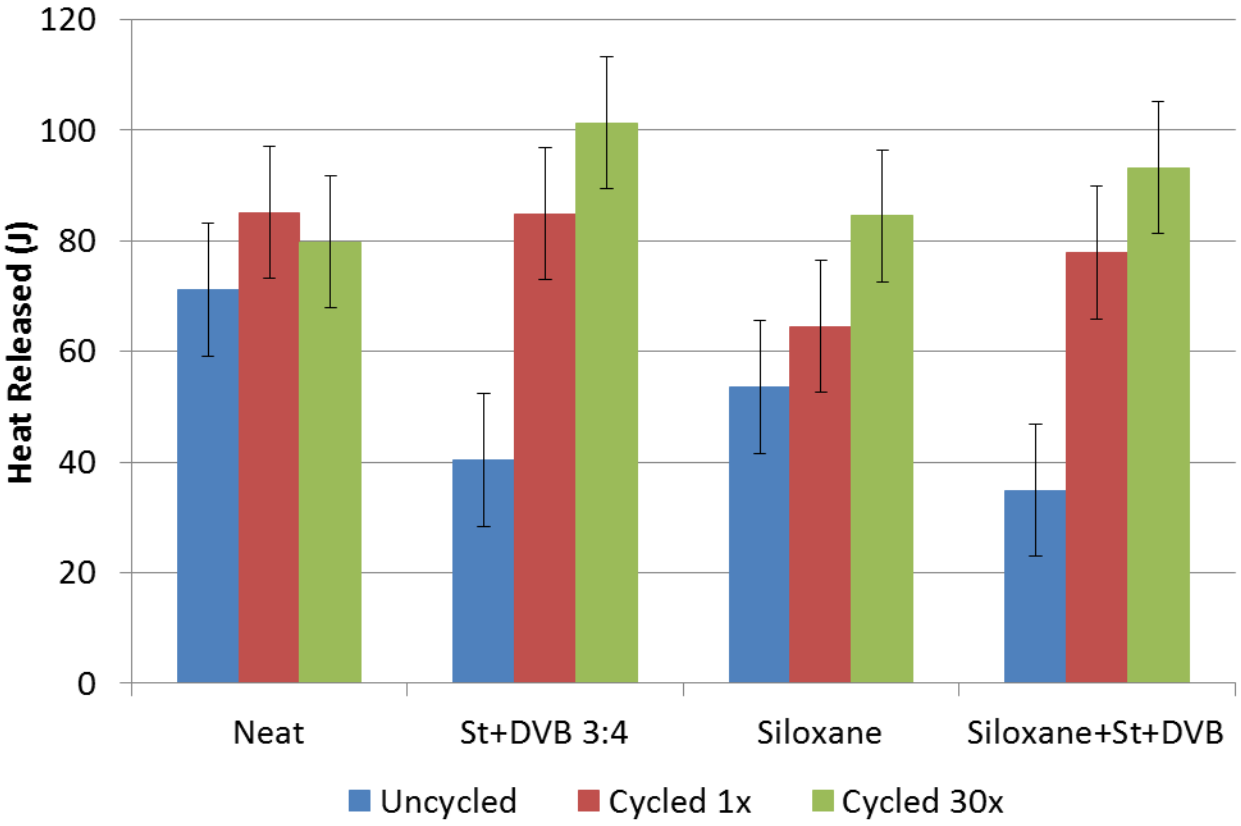

Figure 26: Heat release of the different materials for uncycled and cycled conditions. While the polymer composites mitigate the heat release well in the uncycled material, the mitigating effect is lost upon cycling.

The amount of heat released by the samples is illustrated in Figure 26, which compares the heat release of the neat material with three of the polymer composites for uncycled (blue bars, left), cycled once (red bars, middle) and cycled 30 times (green bars, right). When comparing the Uncycled tests, all of the polymer composites are successful at mitigating the reaction. The styrene/divinylbenzene (St:DVB) 3:4 reduces heat release to 57% of the unmitigated amount, the siloxane to 75%, and the combined siloxane+St:DVB is the best initial performer, reducing heat release to 49% of the unmitigated value. The estimated experimental error is ±11.9 J (± 17% when compared to the unmitigated), so all of these could mitigate to nearly the same level when the error is taken into account.

Comparison of the uncycled to cycled 1x data for the St:DVB-containing composites shows the heat release has more than doubled after cycling just one cycle, indicating that that the mitigating behavior of these composites has greatly diminished. In fact, comparison of the cycled 1x data for these composites to that of the neat material reveals that the mitigating property is completely lost. For the siloxane composite, comparison of the uncycled to the cycled 1x heat release shows a better sustainment of mitigating behavior.

After 30 cycles, all of the composite materials have lost their mitigating ability.

4.4 Durability

Comparison of the capacity results to the heat release results seems to reveal a contradiction with respect to the state of the polymer upon cycling. The hydrogen storage capacity of the composite remains reduced even after 30 cycles, seeming to indicate that the polymer is still present and affecting the metal hydride. But heat release data, showing no mitigating effect after cycling 30 times (and minimal effect after cycling just once), seems to indicate that the polymer is not affecting the metal hydride and is no longer present.

There are different possible explanations for this. One is that the polymer irreversibly affects the hydrogen capacity of the metal hydride, so that even when the polymer is gone the hydride still has a reduced capacity. If this is true, the additive does the exact opposite of our original goal: it adversely affects metal hydride performance without providing any mitigating benefit. Another possibility is that the mitigating and capacity-reducing functions of the additive are separate phenomena, and while cycling eliminates the mitigating function it does not greatly affect the capacity-reducing function. If this is true, it provides an opportunity to discover the mitigating function and perhaps exploit it independently of the capacity-reducing function and/or to discover the phenomenon that allows the capacity-reducing function to remain and either eliminate it or apply it to the mitigating function.

For further insight it is helpful to examine the TGA analysis again. The TGA data given in Figure 25 show that, for the polystyrene materials, the amount of polymer present in the 3:4 material has remained relatively constant up to 180 cycles. Figure 21 showed the same for the siloxane-ps composite material up to 30 hydrogen-sorption cycles. Thus, for both the 3:4 polystyrene and siloxane composites, it appears that the polymer remains in the composite during cycling.

So the TGA testing has revealed that both the sty:DVB 3:4 and siloxane-containing polymers are still present, which is consistent with the cycling capacity results that showed the presence of the polymer depresses the hydrogen capacity in a constant manner throughout the test. Therefore, cycling does not seem to be destroying the polymer itself so much as it is having an adverse effect on just the mitigating function of the polymer. The most plausible, yet unverified, explanation considering all of this information is that the capacity-reducing function of the polymer is a mechanical one, blocking active sites from participating in sorption. In contrast, the mitigating function is a chemical one, and continued exposure to the high pressure, high temperature, and reducing environment of cycling is causing chemical changes in the polymer that eliminates its mitigating ability.

5 Conclusions and Future Work

This chapter presents the overall conclusions of this study and recommends potential future work in the area.

5.1 Conclusions

Polymer/metal-hydride composite materials were synthesized through free radical polymerization of styrene and divinyl benzene in toluene using AIBN as initiator. It was found that vinyl arenes could be polymerized under free-radical polymerization conditions to furnish cross-linked networks in the presence of sodium alanate. Yields for the polymer portion of the composite were slightly lower than neat polymer yields but typically approached 85%.

Consistent with previous work it was found that higher Styrene/divinyl benzene (St/DVB) ratios gave harder/tougher materials compared to more brittle composite materials that formed from lower St/DVB ratios. It is hypothesized that when more DVB is added, the amount of cross-linking increases causing a more brittle network compared to one that has a lower cross-linking density. While the physical properties of the material varied with cross-linking density, the thermophysical properties as measured by TGA were largely independent of cross-linking density.

For siloxane -based materials, a composite with a siloxane-only polymer was found to have poor thermal stability (attributed to poor cross-linking) but the addition of styrene yielded a robust material. A composite material was successfully synthesized using styrene, divinyl benzene, and siloxanes in approximately 4:1:4 ratio by mass.

In all cases, the composite material underwent thermal decomposition starting at a lower temperature than that of its polymer constituent. This indicates that the polymer undergoes a major chemical change when synthesized with the metal hydride. However, both the St/DVB and St/DVB-siloxane polymer composites still exhibited decomposition temperatures higher than that of normal use conditions.

The addition of the mitigating polymer to the metal hydride decreases the hydrogen capacity compared to the unmitigated, neat metal hydride. The effect is postulated to be due to a mechanical blocking of sorption sites. This capacity reduction is independent of the number of adsorption/desorption cycles, except for the case of the siloxane-containing materials (discussed below).

Siloxane-containing composites exhibited a stabilizing effect on capacity reduction, even nullifying the natural cycling-induced capacity reduction of unmitigated metal hydride. It is postulated that a chemical reaction may be responsible for stabilizing the metal hydride.

Low cross-linked polymers were found not to be stable upon cycling which led to mass loss of the polymer. Higher crosslinking is necessary to keep the material intact.

The composites mitigate well initially, reducing heat release to between 49% and 75% of its original amount, but degrade under repeated cycling. Before cycling, the styrene/divinylbenzene (St:DVB) 3:4

reduces heat release to 57% of the unmitigated amount, the siloxane to 75%, and the combined siloxane+St:DVB is the best initial performer, reducing heat release to 49% of the unmitigated value. However, the heat release more than doubled after cycling just one cycle, indicating that that the mitigating behavior of these composites has greatly diminished. After 30 cycles, all of the composite materials have lost their mitigating ability.

It seems reasonable to conclude that the capacity-reducing function of the polymer is a mechanical one, blocking active sites from participating in sorption. In contrast, the mitigating function is a chemical one, and continued exposure to the high pressure, high temperature, and reducing environment of cycling is causing chemical changes in the polymer that eliminates its mitigating ability.

5.2 Future Work

This study has opened the door to other investigations, both directly and indirectly related to mitigation of reactive metal hydrides:

1. In general, we have emphasized first finding a mitigating material, then testing its robustness under realistic use conditions. Future work may approach the problem from the opposite side, by first emphasizing materials which are robust under the cycling environment then testing their mitigating properties.
2. Detailed examination of the chemical interaction between the polymer and the active material during synthesis and during cycling. Gaining this understanding may enable better engineering of the polymer to avoid destruction of its mitigating property upon use. In particular, if verified, the apparent stabilizing effect of the siloxane on the metal hydride's hydrogen storage capacity degradation could be a valuable discovery in its own right.
3. Study of additives other than polymers for hazard mitigation. Examples could include substances that react with oxygen as it enters the bed, inorganic nanoparticles, etc.

References

[1] Dedrick, D. E., Behrens, R., Jr., and Bradshaw, R. W. (2007). "The reactivity of sodium alanates with O2, H2O, and CO2." Report SAND2007-4960, Sandia National Laboratories.

[2] Lohstroh, W., Fichtner, M., and Breitung, W. (2009). "Complex hydrides as solid storage materials: First safety tests." *International Journal of Hydrogen Energy*, 34: (14), 5981-5985.

[3] James, C. W., Cortes-Concepcion, J. A., Tamburello, D. A., and Anton, D. L. (2011). "Environmental reactivity of solid-state hydrogen storage systems: Fundamental testing and evaluation." *International Journal of Hydrogen Energy*, In Press, Corrected Proof.

[4] Anton, D. L., James, C. W., Tamburello, D. A., Cortes-Concepcion, J. A., Gray, J. R., and Brinkman, K. S. (2010). "Environmental Reactivity of Solid State Hydride Materials: Modeling and Testing for Air and Water Exposure." *Advances in Science and Technology*, 72 (5th Forum on New Materials Part A), 219-229.

[5] Tanaka, H., Tokoyoda, K., Matsumoto, M., Suzuki, Y., Kiyobayashi, T., and Kuriyama, N. (2009). "Hazard assessment of complex hydrides as hydrogen storage materials." *International Journal of Hydrogen Energy*, 34: (7), 3210-3218.

[6] Mosher, D. A., Arsenault, S., Tang, X., and Anton, D. L. (2007). "Design, fabrication and testing of NaAlH4 based hydrogen storage systems." *Journal of Alloys and Compounds*, 446-447, 707-712.

[7] Khalil, Y. F., Laube, B., Brown, R., Opalka, S., and Tang, X. (2011). "Quantifying and Addressing the DOE Material Reactivity Requirements with Analysis and Testing of Hydrogen Storage Materials and Systems." *DOE Hydrogen and Fuel Cells Program and Vehicle Technologies Program Annual Merit Review and Peer Evaluation Meeting*, Arlington, VA, May 9-13.

[8] Dedrick, D. E. (2007). "Safety Properties of Hydrogen Storage Materials." *2007 Annual Progress Report*, U.S. Department of Energy, 635-637.

[9] Dedrick, D., Behrens, R., Kanouff, M., Bradshaw, B., Larson, R., and Evans, G. (2008). "Chemical and Environmental Reactivity Properties of Hydrogen Storage Materials within the Context of Systems." *2008 Annual Progress Report*, U.S. Department of Energy, 748-753.

[10] Dedrick, D., Behrens, R., Kanouff, M., Bradshaw, R., Cordaro, J., and Whinnery, L. (2009). "Chemical and Environmental Reactivity Properties of Hydrogen Storage Materials within the Context of Systems." *2009 Annual Progress Report*, U.S. Department of Energy, 729-734.

[11] Dedrick, D. E., Kanouff, M., Larson, R., Bradshaw, B., Sartor, G., Behrens, R., Whinnery, L., Cordaro, J., and Highley, A. (2009). "The reactivity properties of hydrogen storage materials in the context of systems." *2009 U.S. Department of Energy (DOE) Hydrogen Program and Vehicle Technologies Program Annual Merit Review and Peer Evaluation Meeting*, Arlington, VA, May 18-22.

[12] Dedrick, D., Behrens, R., Kanouff, M., Bradshaw, R., Cordaro, J., Pratt, J., and Reeder, C. (2010). "The Reactivity Properties of Hydrogen Storage Materials in the Context of Systems." *2010 Annual Progress Report*, U.S. Department of Energy, 586-590.

[13] Dedrick, D. E., Cordaro, J. G., Kanouff, M. P., Bradshaw, R. W., and Khalil, Y. F. (2010). "Mitigating hazards during accident scenarios involving metal hydride materials." *2010 National Hydrogen Association Conference and Expo*, Long Beach, CA, May 2-4.

[14] Dedrick, D. E., Kanouff, M., Cordaro, J., Reeder, C., Bradshaw, B., Sartor, G., and Keller, J. (2010). "The reactivity properties of hydrogen storage materials in the context of systems." *2010 U.S. Department of Energy (DOE) Hydrogen Program and Vehicle Technologies Program Annual Merit Review and Peer Evaluation Meeting*, Washington, D.C., June 7-11.

[15] Dedrick, D. E., Cordaro, J. G., Kanouff, M. P., Reeder, C. L., Pratt, J. W., and Khalil, Y. F. (2010). "Mitigation Technologies for Hydrogen Storage Systems based on Reactive Solids." *AIChE Annual Meeting*, Salt Lake City, UT, November 8-12.

[16] Pratt, J. W., Cordaro, J. G., Reeder, C. L., Kanouff, M. P., Ruvalcaba Jr., I., and Dedrick, D. E. (2011). "Composite Materials for Hazard Mitigation of Reactive Metal Hydrides." *2011 DOE Hydrogen and Fuel Cells Program and Vehicle Technologies Program Annual Merit Review and Peer Evaluation Meeting*, Arlington, VA, May 9-13.

[17] Dedrick, D. E., Kanouff, M. P., Replogle, B. C., and Gross, K. J. (2005). "Thermal properties characterization of sodium alanates." *Journal of Alloys and Compounds*, 389: (1-2), 299-305.

[18] Dedrick, D. E., Kanouff, M. P., Larson, R. S., Johnson, T. A., and Jorgensen, S. W. (2009). "Heat and mass transport in metal hydride based hydrogen storage systems." *Proceedings of HT2009, ASME Summer Heat Transfer Conference*, San Francisco, CA, July 19-23, ASME.

[19] Currie, J. A., and Dole, M. (1969). "Specific heat of synthetic high polymers. XIII. Amorphous polystyrene." *The Journal of Physical Chemistry*, 73: (10), 3384-3389.

[20] Henderson, J. B., and Emmerich, W. D. (1991). "Measurement of specific heat and energetic characterization of materials up to high temperatures." *Journal of Thermal Analysis and Calorimetry*, 37: (8), 1979-1985.

[21] Kuo, A. C. M. (1999). "Poly(dimethylsiloxane)." *Polymer Data Handbook*, J. E. Mark, ed., Oxford University Press, New York, 411-435.

[22] Bartholomew, C. H., and Farrauto, R. J. (2006). *Fundamentals of Industrial Catalytic Processes*, John Wiley & Sons, Hoboken, NJ.

Appendix A: Method of Calculating $Q_{surroundings}$

Although the heat lost to the surroundings was found to be negligible, the analysis method for finding this quantity is presented here.

The heat released by the reaction that is lost to the surroundings, $Q_{surroundings}$, is calculated based on an empirical correlation developed by a dedicated heat loss test run. This was deemed to be easier and just as accurate as attempting to calculate the convective and radiative heat transfer from theory because of the typical uncertainty of those methods (due to estimating emissivities, convection coefficients (±20% uncertainty contribution alone), Nussalt correlations, etc.)[1] and the fact that the conditions surrounding our test are consistent for each run. To calculate $Q_{surroundings}$ as a function of time, Newton's Law of Cooling says:

$$\dot{Q}_{surroundings}(t) = hA(T(t) - T_{Ambient}) \tag{12}$$

Here, we are using *hA* to represent the overall heat transfer coefficient from the vessel to the surroundings; that is, it includes the effects of convection and radiation. It can also be derived that[2]:

$$\frac{T(t) - T_{Ambient}}{T_{initial} - T_{Ambient}} = e^{-bt} \tag{13}$$

where:

$$b = \frac{hA}{mC_{p,solid}} \tag{14}$$

m is the mass of the sample, and is measured. Equations (12) and (14) can be combined and summed over each time step (Δt) to find the total amount of heat lost to the surroundings during the test:

$$Q_{surroundings} = bmC_p(T(t) - T_{Ambient})\Delta t \tag{15}$$

All quantities are measurands except for *b*. Equation (13) can be rearranged to:

$$T(t) - T_{Ambient} = (T_{initial} - T_{Ambient})e^{-bt} \tag{16}$$

Then, plotting the quantity ($T(t)$-$T_{Ambient}$) vs. time will allow curve fitting to the exponential equation with y-intercept ($T_{initial}$-$T_{Ambient}$), thus finding the value of *b* for our experiment. The heat loss experiment's result and the curve fit are shown in Figure 27. The value of *b* is determined to be 0.0006611. In the region we are interested in, that is, for $T(t)$ > 200 °C, this heat loss prediction method gives a maximum error of 7.8% compared to the measurement.

[1] Cengel, Y. A. (2003). *Heat Transfer: A Practical Approach, Second Edition*, McGraw-Hill, New York NY.
[2] *Ibid*.

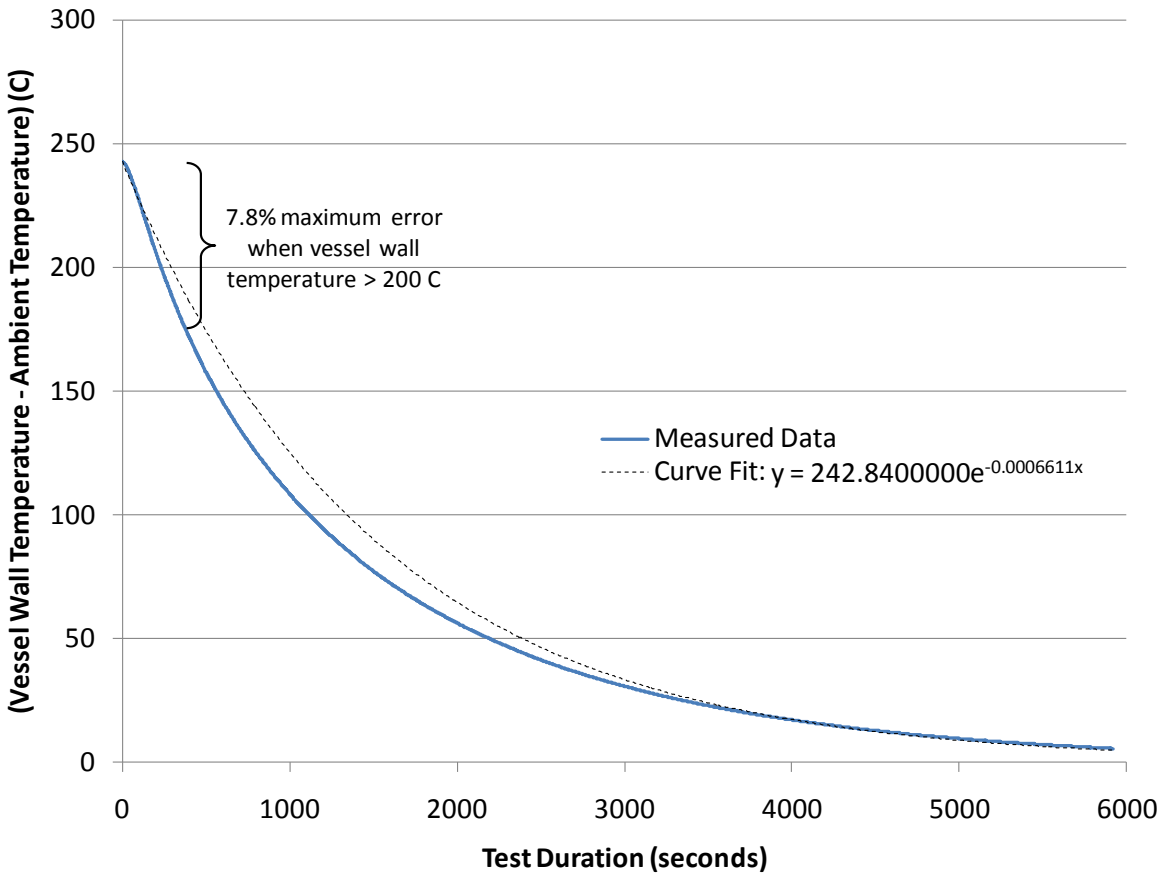

Figure 27: Heat loss test result, used to estimate the amount of heat lost to the surroundings during an oxidation. The exponential constant 0.0006611 is used for *b* in Eq. (15). It can be seen by the non-coincident curve fit that actual heat loss is slightly greater than estimated by this method.

Distribution

2 U.S. Department of Energy
Attn: Ned Stetson
1000 Independence Ave., SW
Washington, D.C. 20585-0121

1	MS9051	Neal Fornaciari	08366 (electronic copy)
1	MS9052	Daniel Dedrick	08367
1	MS9054	Bob Carling	08300 (electronic copy)
1	MS9054	Art Pontau	08360 (electronic copy)
1	MS9161	George B. Sartor	08366
1	MS9403	Joseph G. Cordaro	08223
1	MS9409	Joseph W. Pratt	08366
1	MS0899	Technical Library	9536 (electronic copy)


Sandia National Laboratories